
Earthquake Source Parameters, Rapid Estimates for Tsunami Forecasts and Warnings



Barry Hirshorn¹, Stuart Weinstein², Dailin Wang², Kanoa Koyanagi², Nathan Becker² and Charles McCreery²

¹NOAA/NWS, Ewa Beach, HI, USA

²NOAA/NWS/Pacific Tsunami Warning Center, Ewa Beach, HI, USA

Article Outline

Glossary

Definition of the Subject

Introduction

Tsunami Warning Center Operations

Seismic Methods

Earthquake Source Parameters

Future Directions

Bibliography

Glossary

CMT centroid moment tensor The CMT represents properties of the earthquake source derived from the seismic displacement of the Earth's crust that best reproduces the observed wave field generated by an earthquake and gives the average location in time and space of the earthquake energy release. The scalar seismic moment can be determined from the CMT.

Convolution A type of integral transform combining two signals to form a third signal or output. The output signal is typically viewed as a modified version of one of the two original signals, giving the area overlap between the two signals as a function of one of the original signals is translated with respect to the other. It is the single most important technique in digital signal processing. In the case of seismology, the two signals can be, e.g., the ground motion

as a function of time and the response of the seismometer, and the output is the seismogram.

Deconvolution Does the reverse of convolution. In the case of seismology, one uses deconvolution to remove the instrument response from the seismogram to recover the actual ground motion.

Deep earthquake An earthquake characterized by a hypocenter located more than 100 km below the Earth's surface.

Hypocenter The point within the Earth where the earthquake rupture starts. The epicenter is the projection of the hypocenter onto the Earth's surface.

Local tsunami warning A tsunami warning for distances less than 100 km from the source.

Magnitude

- | | |
|----|---|
| mB | The “broadband” body-wave magnitude, generally based on measurements of the amplitude of P-waves with periods in the 2 to 20 s range. |
| MS | The surface wave magnitude. MS is generally based on measurements of the amplitude of the surface (Love or Rayleigh) waves with periods of about 20 s. The US tsunami warning centers have applied a correction to the IASPEI formula that allows the estimation of MS closer to the epicenter at a period near 20 s. |
| ME | The “energy-magnitude” scale, derived from velocity power spectra. |
| Mm | The mantle wave magnitude, based on the measurement of the amplitude of surface waves with periods of 50–400 s. |

MW	The moment magnitude, based on the estimation of the scalar seismic moment, M_0 .		P-wave that travels downward from the epicenter and reflects once off of the surface. The definitions of the S-wave phases follow in the same manner.
Mwp	The moment magnitude based on the initial long-period P-waves.		
ML	The local magnitude scale, based on the measurement of the maximum peak-to-peak amplitude observed on a Wood-Anderson seismogram, corrected for the decrease in amplitude with increasing epicentral distance. Generally based on the analysis of Sg, Lg, or Rg surface waves oscillating with periods observed out to 600 km from the earthquake's epicenter.	Seismic moment	The seismic moment, M_0 (expressed in units of force times distance, e.g., Newton-meters or dyne-cm), is the moment of either couple of an equivalent double couple point source representation of the slip across the fault area during the earthquake. Mathematically, the seismic moment, $M_0 = \mu Ad$, where μ denotes the shear rigidity or resistance of the faulting material to shearing forces, A represents the area of the fault plane over which the slip occurs, and d represents the average coseismic slip across A .
pMag	A magnitude scale based on the average of the absolute values of the first three half cycles of the P-waves recorded at local distances.		
Marigram	A recording of sea-level variations obtained by tide gauges.	Seismic waves	Elastic waves generated by movements of the earth's crust that propagate as radiated seismic energy, ER.
Regional tsunami warning	A tsunami warning for distances up to 1000 km from the source.	Seismic surface waves	Waves that propagate along the surface boundary of a medium, e.g., along the surface of the earth.
Seismic body waves	Waves that propagate through the interior of an unbounded continuum. Primary waves (P-waves) are longitudinal body waves that shake the ground in a direction parallel with the direction of travel. Secondary body waves (S-waves) are shear waves that shake the ground in a direction perpendicular to the direction of travel. There are other types of arrivals (also known as phases) visible on seismographs corresponding to reflections of P- and S-waves from the earth's surface: The pP phase is a P-wave that travels upward from the hypocenter and reflects once off the surface, and the PP phase is a	Shallow earthquake Teletsunami warning Tsunami	An earthquake characterized by a hypocenter located within 100 km of the Earth's surface. A tsunami warning for distances greater than 1000 km away from the source. A series of water waves generated by any rapid, large-scale disturbance of the sea. Most tsunamis are generated by seafloor displacements from large undersea earthquakes, but they can also be caused by large submarine landslides, volcanic eruptions, calving of glaciers, and even by meteorite impacts into the ocean.

Tsunami earthquake	An earthquake that generates a much larger tsunami than expected given its magnitude.
Tsunami warning system	A tsunami warning system consists of a tsunami warning center such as the Pacific Tsunami Warning Center (PTWC), a formal response structure that includes civil defense authorities and government officials, and an education program that brings a minimum level of awareness and education to the coastal populations at risk.
W-phase	A distinct long-period, up to 1000 s, phase which arrives before the S phase. Kanamori (1993) first observed it on the displacement records of the 1992 Nicaragua tsunami earthquake. The W-phase is so-called because it propagates in a manner similar to that of the acoustic whispering gallery mode (Kanamori 1993).

As fast as tsunami waves are, seismic waves travel at speeds more than 40 times greater. Because of this large difference in speed, scientists rely on seismic methods to detect the possibility of tsunami generation and to warn coastal populations of an approaching tsunami well in advance of its arrival. Seismic P-waves, for example, travel from Alaska to Hawaii in approximately 7 min, whereas a tsunami takes about 5½ h to travel the same distance. Although over 200 sea-level stations, reporting in near real time, are operating in the Pacific, it may take an hour or more, depending on the location of the epicenter, before the existence (or not) of an actual tsunami is confirmed. In other ocean basins where the density of sea-level instruments reporting data in near real time is less, the delay in tsunami detection is correspondingly longer. In addition, global, regional, and local seismic networks, and the infrastructure needed to process the large amounts of seismic data that they record, are widespread. For these reasons, tsunami warning centers provide their initial tsunami warnings to coastal populations based entirely on seismic data.

Definition of the Subject

Tsunamis are among nature's most destructive natural hazards. Typically generated by large, underwater earthquakes near the Earth's surface, tsunamis can cross an ocean basin in a matter of hours. Although difficult to detect, and not dangerous while propagating in deep water, tsunamis can unleash immense destructive power when they reach coastal areas. With advance warning, coastal populations can be alerted to move to higher ground and away from the coast, saving many lives. Unfortunately, due to the lack of a tsunami warning system in the Indian Ocean, the Sumatra earthquake and tsunami of Dec. 26, 2004, killed over 250,000 people, with thousands of lives lost as far away as East Africa many hours after the earthquake occurred. Had a tsunami warning system been in place, many lives could have been saved.

Introduction

Any mechanism that causes a sudden displacement of the ocean's surface affecting a significant volume of water can produce a tsunami. Undersea earthquakes, landslides, volcanic explosions, calving of icebergs, and even meteorite impacts can generate tsunamis. However, the majority of tsunamis are generated by earthquakes. Not uncommon are earthquakes that trigger landslides, so that both the displacement of the crust due to the earthquake and the landslide each contribute to the generation and size of the tsunami. Tsunamis are a devastating natural, high fatality hazard (Bryant 2001). In the absence of a proper tsunami warning system, a destructive tsunami will cause death and destruction as it encounters coastal areas while propagating across an entire ocean basin as it did in the case of the Sumatra tsunami of December 2004.

Although tsunamis propagate in deep water with speeds exceeding 900 km/h, they are hard

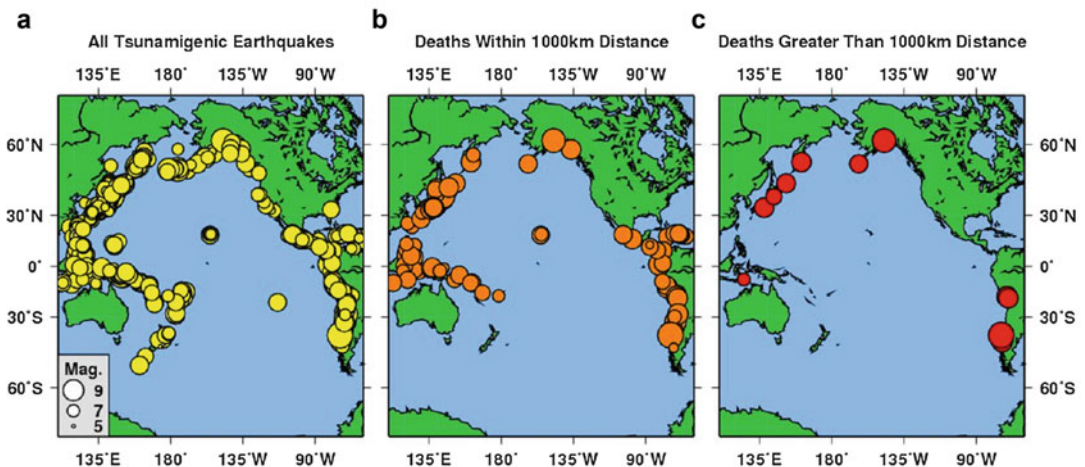
to detect in the open ocean. For example, the first wave of the great 2004 Sumatra tsunami had a wave height of only 1 m in deep water (depth > 500 m) (Gower 2005) and a wavelength on the order of several hundred kilometers. Consequently, people aboard ocean vessels did not feel the accelerations caused by the tsunami as it passed under them. However, as the speed, v (in m/s), of a tsunami is governed by the simple relation $v = \sqrt{gh}$, where g is the acceleration of gravity (in m/s^2) and h is the thickness of the water column (in m), the tsunami will slow down as it propagates into shallow water. At this point, the wave speed and wavelength decrease, causing the wave height to increase. Depending on the nature of the tsunami, and the shape and bathymetry of the coastal area, the tsunami wave height can be greatly amplified, magnifying its destructive power.

Because earthquakes generate most tsunamis, and seismic waves travel more than 40 times faster than tsunamis, the first indication that a tsunami may have been generated is the earthquake itself. Depending on the earthquake's location (undersea or inland), depth (shallow or deep) in the Earth's crust, and on its magnitude, a

tsunami warning center may issue an official message product. If the earthquake is a shallow, undersea earthquake, the severity indicated by the initial message will depend upon the magnitude of the earthquake. The more rapidly and accurately the tsunami warning center can characterize the earthquake source, the faster it can make the initial evaluation of the tsunamigenic potential of the earthquake.

While some tsunamis are destructive, most are rather small, producing few if any casualties and little or no damage, although they are easily observable on marigrams (Fig. 1). On the basis of how widespread their effects are, tsunamis can be classified as local (within 100 km of the epicenter), regional (up to 1000 km from the epicenter), or teletsunamis (greater than 1000 km from the epicenter). Warning centers designed to respond to tsunami threats on each of these scales now exist in every major ocean basin.

The Pacific Tsunami Warning Center (PTWC) provides basin-wide warnings to the coastal areas of the Pacific and Caribbean basins. The PTWC also functions as a local tsunami warning center for Hawaii, Puerto Rico, the Virgin Islands, Guam, and American Samoa. Other local



Earthquake Source Parameters, Rapid Estimates for Tsunami Forecasts and Warnings, Fig. 1 Epicenters of tsunamigenic earthquakes occurring in the Pacific since 1 A.D. Of those earthquakes that do produce a tsunami (a), most tsunamis cause no damage. Most events that cause casualties and/or damage do so within 1000 km of the

epicenter (b), leaving only a few great earthquake sources that generated tsunamis which caused casualties and/or damage more than a 1000 km from the epicenter. (c) Data provided by the NOAA National Geophysical Data Center (NGDC) (www.ngdc.noaa.gov/hazard/tsu.html)

Tsunami warning centers include the CPPT (French Polynesia Tsunami Warning Center), which is based in Tahiti, GFZ-Indonesia, which is based in Jakarta which provides local warnings for Indonesia, and Japan's JMA (Japan Meteorological Agency) which provides local tsunami warnings to Japan. Examples of regional warning centers include the Japan Meteorological Agency (JMA), which provides regional tsunami warnings to the Northwest Pacific, and the National Tsunami Warning Center (NTWC), which provides regional warnings to the US mainland coasts and the west coast of Canada.

The tsunami warning centers themselves are not complete tsunami warning systems; they are simply the first line of defense within these warning systems. A tsunami warning system consists of three main components: (a) the tsunami warning center, (b) the emergency management/civil defense authorities who receive tsunami warning center message products and mobilize the public, and (c) the coastal populations themselves, who must be educated on how to respond to tsunami emergencies. If any of these three components are lacking, the tsunami warning system will fail. Unfortunately, none of these components existed in the Indian Ocean at the time of the December 2004 Sumatra earthquake and tsunami. However, in the decade since this disaster, Indonesia, Australia, and India have created tsunami warning systems in the Indian Ocean basin.

The greatest challenge for a tsunami warning system, particularly in the near field, is rapid identification of slow (in terms of fault rupture speed) "tsunami" earthquakes. Tsunami earthquakes are so-called because they generate much larger tsunamis than expected from their magnitude (Kanamori 1972). In a well-functioning tsunami warning system, residents in coastal areas are educated to immediately move inland, and onto higher ground if they feel strong ground shaking, and not wait for an official tsunami alert (Fryer et al. 2005). However, because a tsunami earthquake produces much less radiated high-frequency energy than normal, even a large (in terms of moment magnitude) tsunami earthquake may not be strongly felt in the near field, so that this strategy of having people self-evacuate upon feeling strong ground

shaking will not work. This was, unfortunately, made clear by the Java "Tsunami" earthquake of July 17, 2006. The tsunami generated by this earthquake killed at least 500 people, as many residents in coastal areas near the earthquake did not feel strong shaking (Widjo et al. 2006). Tsunami warning centers need to be able to properly detect the occurrence of these tsunami earthquakes as soon as possible after they begin.

Tsunami Warning Center Operations

Tsunami warning centers function much like seismic observatories in detecting, locating, and characterizing earthquakes, with the difference that they are primarily interested in very large earthquakes and that their earthquake parameterization needs to be very fast, sometimes sacrificing precision. Depending on the earthquake's location (underwater vs. inland), depth below the surface, and magnitude, tsunami warning centers may issue an official message product to advise emergency management authorities within the warning center's AOR (area of responsibility) of the occurrence of a large earthquake and its potential for generating a tsunami. The PTWC, located in Honolulu, Hawaii, provides such notice regarding the potential or confirmed generation of a destructive tsunami for most of the Pacific Ocean and Caribbean Sea and their adjacent seas. The PTWC also provided tsunami threat information for the Indian Ocean basin following the December 26, 2004, Indian Ocean tsunami until the end of April 2013.

PTWC's international message products and criteria were substantially changed in 2014, after several years of consultation with and training of the Pacific Tsunami Warning System (PTWS) Member States. The new products were created in an effort to reduce the amount of over-warning and to give more authority to the disaster management organizations of the Member States to formulate what specific alerts and actions to take along their coastlines. Among the important changes are the adoption of new terminology that provides threat levels instead of alert levels like "warning" or "watch" and the inclusion of tsunami wave amplitude forecasts in the message

products. Under the new guidelines, the first bulletin issued assesses the potential of the earthquake to generate a destructive tsunami based solely on the earthquake location, depth, and magnitude, just as the previous products did. However, after PTWC obtains a reliable CMT, about 25 minutes post origin time, subsequent products base tsunami threat levels on forecasted and observed wave heights. The following provides a general description of PTWC's products for the Pacific.

Observatory Message: The PTWC sends an observatory message to certain seismological observatories and organizations for any earthquake with a magnitude of about 5.8 or greater. In areas with dense seismic networks, the PTWC may issue an observatory message for earthquakes as small as magnitude 4. This unofficial message contains only the earthquake's preliminary epicentral location, origin time, depth, magnitude, and a list of stations used in computing these parameters. These messages contain no evaluation regarding the seismic or tsunami hazard.

Tsunami Information Statement: The PTWC issues this message product for any earthquake in the vicinity of the Pacific basin with a magnitude in the range $6.5 \leq M_w \leq 7.0$ or for larger earthquakes when they are located too far inland or too deep inside the earth to pose a tsunami threat.

Tsunami Threat Message: The PTWC issues this message product for any shallow (depth < 100 km) undersea or nearshore earthquake in or near the vicinity of the Pacific basin with a magnitude $M_w \geq 7.1$. If the magnitude is in the range $7.1 \leq M_w \leq 7.5$, the tsunami threat message will indicate a possible tsunami threat to coasts located within 300 km of the epicenter. If the magnitude is in the range $7.6 \leq M_w \leq 7.8$, the tsunami threat message will indicate a possible tsunami threat to coasts located within 1000 km of the epicenter, and finally, if the magnitude is $M_w \geq 7.9$, the tsunami threat message will indicate a possible tsunami threat to coasts located within 3 h tsunami travel time of the earthquake's epicenter.

After a reliable CMT is obtained, subsequent tsunami threat messages will place coastlines in "threat levels" based on the maximum forecast wave heights generated by RIFT (see section on "Real-Time Tsunami Forecasting") and any sea-level observations that are available. The threat levels assigned to a coastline are described below:

1. No threat: Maximum forecast wave amplitude is below 30 cm.
2. Maximum forecast wave amplitude (H) is in the range $30 \text{ cm} \leq H < 1 \text{ m}$.
3. Maximum forecast wave amplitude (H) is in the range $1 \text{ m} < H \leq 3 \text{ m}$.
4. Maximum forecast wave amplitude greater than 3 m.

In general, threat level 2 indicates the possibility of dangerous offshore currents as well as some flooding of beaches and harbors. Threat levels 3 and 4 generally indicate an inundation hazard, with level 4 indicating the possibility of extensive inundation along the coast by the tsunami.

Supplemental tsunami threat messages are issued with updated sea-level observations and other information until the tsunami hazard has generally passed at which time a final tsunami threat message is issued.

In consultation with the Caribbean tsunami warning system (CARIBE-EWS), the PTWC also issues the following products for the Caribbean Ocean basin:

Tsunami Information Statement: The PTWC issues this message product for any earthquake in the vicinity of the Caribbean Sea, with a magnitude in the range $6.0 \leq M_w \leq 7.0$, or in the Atlantic with a magnitude in the range $6.5 \leq M_w \leq 7.8$ or for larger Caribbean or Atlantic earthquakes when they are located too far inland or too deep inside the earth to pose a tsunami threat.

Tsunami Threat Message: Tsunami threat messages issued for the Caribbean Ocean basin or Atlantic Ocean basin are similar, and the magnitude criteria and threat levels are the same as in the above paragraph describing the Pacific Ocean basin tsunami threat messages.

Coastlines close to the earthquake epicenter can experience tsunami waves within 2 to 30 min after the earthquake; hence a local tsunami warning needs to be issued within a few minutes to be effective. This requires access to real-time data provided by a dense local network of seismic stations near the epicenter to allow both the rapid location and source characterization of the earthquake. In the case of the Hawaii region, the PTWC uses data from its own local seismic network and from the dense seismic network maintained by the USGS Hawaii Volcano Observatory (HVO) to rapidly detect and characterize local Hawaii earthquakes. These data, combined with automatic local Earthquake detection, association, and paging based on initial p-wave magnitude estimations, introduced at the PTWC in 1999–2000 (Allen 1978, 1982; Johnson et al. 1994, 1995; Hirshorn et al. 1993) enabled the PTWC to issue an information bulletin to the state of Hawaii and to the Pacific basin, for the October 15, 2006, Kiholo Bay earthquake (M_w 6.7) within 3 min of the origin time of the earthquake (Hirshorn 2007) (Fig. 2b). However, the PTWC cannot issue timely local Tsunami warnings for populations in the immediate vicinity of large earthquakes outside of Hawaii, Puerto Rico, or the Virgin Islands because PTWC lacks access to dense enough local seismic networks outside of these regions (Fig. 2a).

Japan maintains an extremely dense seismic network and can therefore rapidly issue warnings for offshore earthquakes. Spurred on by the December 2004 Sumatra and Chile 2010 earthquakes, several other nations such as Indonesia, Australia, Chile, and New Zealand, for example, have all rapidly developed their seismic networks in an effort to improve their local tsunami warning capabilities for earthquakes along their shores.

Seismic Methods

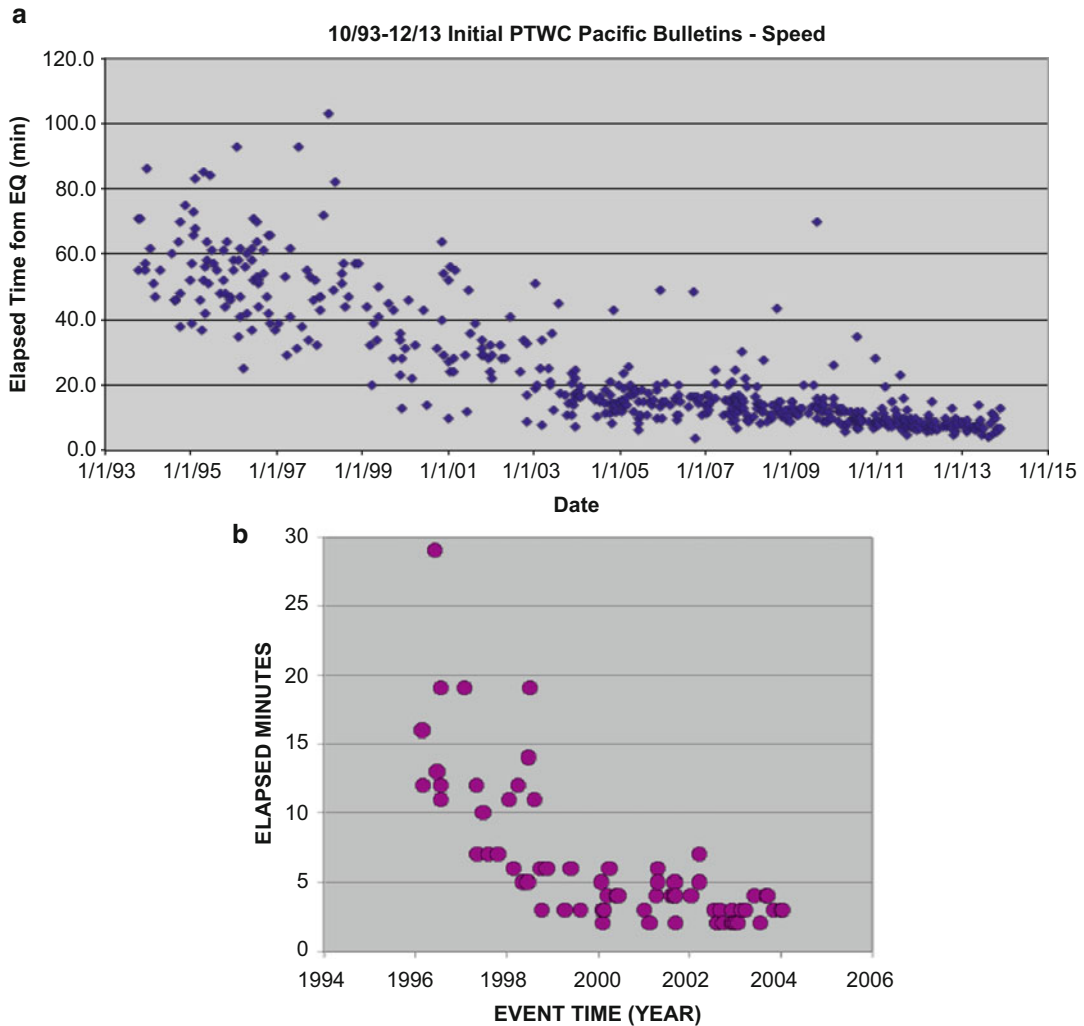
To rapidly detect, locate, and characterize the source of earthquakes occurring around the world, tsunami warning centers rely on the Global Seismic Network (GSN USGS/IRIS), the USGS/NEIC, and a number of other seismic data contributors worldwide. It is this unfettered access to

real-time seismic data supplied by a number of different networks that makes basin-wide tsunami warning centers possible. To rapidly deal with the threat posed by locally generated tsunamis to the state of Hawaii, PTWC processes seismic data from about 80 stations located throughout the Hawaiian Islands. The USGS HVO's dense seismic network supplies most of this data. The US tsunami warning centers use the Earthworm software developed by the USGS to import and export seismic data (Johnson et al. 1995).

PTWC duty scientists receive automatic pages within a few minutes of the beginning of any earthquake with a M_w of approximately 5.5 or greater. The system generating these pages uses Evan's and Allen's (1983) teleseismic event detection algorithm, adapted for broadband data by Wither's (1998) and Whitmore's and Blackford's (2002) teleseismic picker (which picks the first p-wave arrival time) and phase associator (which associates those arrival times belonging to a single earthquake together). In the Hawaiian Islands, Puerto Rico, and the Virgin Islands, Earthworm (Johnson et al. 1995) automatically notifies duty scientists of earthquakes with magnitudes larger than 3.5 within 10 to 20 s of the earthquake's origin time, locates the hypocenter, and provides a first estimate of the earthquake's magnitude and other source parameters in real time (Allen 1978, 1982; Johnson et al. 1994, 1995). PTWC duty scientists then refine and supplement the automated real-time hypocenter location and/or magnitude estimates. Determining the earthquake's depth is particularly important as earthquakes occurring at depths greater than 100 km generally do not cause dangerous tsunamis.

Earthquakes are located using P-wave arrival times recorded at a number of seismic instruments. As both the locations of seismic instruments and P-wave travel times as a function of distance are well known, a process analogous to triangulation is used to locate the earthquake. The pickers and associators perform these functions automatically on a continuous basis.

While the depth of the earthquake can be estimated on the basis of P-times alone, a more robust result often requires the addition of depth phases such as pP, which is a P-wave that travels directly



Earthquake Source Parameters, Rapid Estimates for Tsunami Forecasts and Warnings, Fig. 2 Elapsed time from earthquake origin time to time of issuance of the first official message product for (a) teleseisms (earthquakes

that occur outside of the Hawaiian Islands region) and (b) for earthquakes that occur within the Hawaiian Islands. The PTWC's mean time after origin for Pacific Bulletins has been 5–6 minutes from 2017 through 2018

up to the earth's surface from the earthquake source and reflects once off of that surface before arriving at the seismometer. The duty scientists use pP arrival times to refine hypocentral depths of distant earthquakes (teleseisms). For earthquakes in Hawaii, Puerto Rico, and the Virgin Islands, observed at local distances, the S-wave arrival time would be useful for constraining earthquake depth.

Seismologists use a panoply of different magnitude scales to characterize the seismic source. These different methods examine different parts

of the seismic wave train, such as short- and long-period body waves (seismic waves that travel through the earth's interior like the P- and S-waves) and longer-period surface waves (slower seismic waves that are constrained to travel along the earth's surface). Most of these magnitude scales were developed to estimate the energy released by the earthquake as radiated seismic wave energy, E_R . Traditional magnitude measures such as M_L (Richter 1935) and m_b (a shorter-period variant of m_B Gutenberg (1945c; Gutenberg and Richter 1956a)) examine

high-frequency body waves. Gutenberg's surface wave magnitude M_S (Gutenberg 1945a; Vanek et al. 1962) is derived from longer-period surface waves. A relatively new and quick method, M_{wp} , analyzes long-period P-waves (Tsuboi et al. 1995, 1999; Whitmore et al. 2002). The M_{wp} magnitude now provides the basis used to decide which, if any, official message product to issue, replacing the M_S method that the PTWC had been using for over 50 years. For large earthquakes, duty scientists also routinely estimate the mantle magnitude M_m , a very long-period surface wave magnitude based on mantle waves with periods in the range 50–410 s (Okal and Talandier 1989). The relationship between these magnitudes, each looking at different parts of the seismic wave spectrum of an earthquake, can be used to characterize the earthquake source (Aki 1967; Brune 1970, 1971; Kanamori 1977, 1978, 1983; Kanamori and Kikuchi 1993).

Today, the PTWC's best estimate of M_W comes from the inversion of the W-phase to obtain the CMT (Kanamori and Rivera 2008). The W-phase CMT calculation is triggered by any PTWC preliminary earthquake message for an earthquake with magnitude >6.8 . A W-phase-based CMT and M_W are then available within ~ 25 min after the earthquake origin time. The PTWC is testing a regional WCMT which will cut the time required to obtain a robust CMT down to 15 minutes. The PTWC expects to operationalize the regional WCMT in early 2020.

When evaluating the tsunamigenic potential of an earthquake, PTWC duty scientists compute the quantity $\log_{10}(E_R/M_0)$, known as "theta" Θ , where E_R is the radiated energy carried by the high-frequency p-waves and M_0 is the seismic moment (Aki 1966). Newman and Okal (1998) showed that Θ is anomalously small for tsunami earthquakes.

Since the mid-1990s, both US tsunami warning centers response times to potentially tsunamigenic teleseisms have decreased dramatically due to the much larger amounts of seismic data that they now receive and to the switch from the slower M_S magnitude method to the faster and more accurate M_{wp} moment magnitude method as the basis for issuing messages (Fig. 2a). Improved data analysis methods and increased amounts of local seismic data have also significantly decreased the PTWC's

response time to earthquakes occurring in the Hawaiian Islands region (Fig. 2b).

Earthquake Source Parameters

A fundamental problem with traditional magnitude estimates, such as M_L , m_b , and M_S , is that they are based on the amplitudes of relatively short-period seismic waves, with periods usually less than 3 s for m_b and M_L and 20 s for M_S . When the largest rupture dimension of the earthquake exceeds the wavelength of these seismic waves, which, for example, is about ~ 50 km for the 20 s period surface waves used for M_S (Kanamori 1977, 1978, 1983), these magnitude values will start to "saturate." Saturation in this case means that these magnitude methods will underestimate M_w when the periods of the waves on which they are based are shorter than the corner period of the earthquake's seismic wave spectrum (Aki 1967; Brune 1970, 1971) (see Fig. 3).

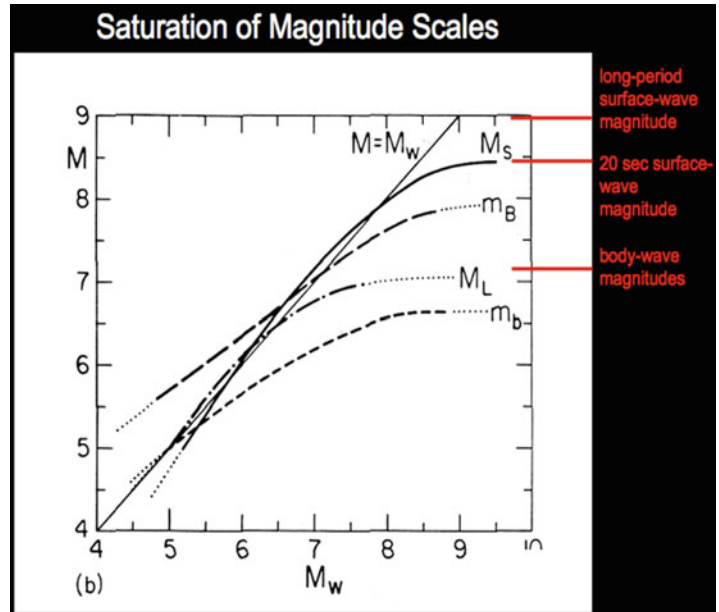
Another equivalent explanation is that these magnitude methods, which look at waves with periods of a fraction of a second to a few tens of seconds, cannot sample enough of the energy released by an earthquake whose source duration (the length of time over which the rupture occurs) is many times longer than the periods used by these methods. As the earthquake becomes very large, one must examine longer-period waves to avoid saturation.

K. Aki used a spectral representation to establish that earthquakes of varying size had similarly shaped spectra, differing primarily in their low-frequency amplitudes, proportional to seismic moment, and in the location of a given spectra's "characteristic frequency" (corner frequency of the source spectrum) (Aki 1967). He related this corner frequency to the characteristic length scale of the earthquake's rupture area (Aki 1967). Brune (1970, 1971) and Savage (1972) also related the corner frequency to the dimensions of the fault plane.

To circumvent the saturation problem, Kanamori defined the moment magnitude M_W (Kanamori 1977), in terms of a minimum estimate of the total coseismic strain energy drop, W_0 , via

Earthquake Source Parameters, Rapid Estimates for Tsunami Forecasts and Warnings, Fig. 3

Saturation of different classical magnitude scales with respect to non-saturating moment magnitude according to Kanamori. Note that m_B refers to the original Gutenberg-Richter (1945b, c) body-wave magnitude scale based on amplitude measurements made on medium-period broadband instruments. It saturates at larger magnitudes when compared to the short-period-based m_b



Gutenberg and Richter's energy-magnitude relationship (Gutenberg and Richter 1956b). M_w measures the work required to rupture the fault, as computed from the seismic moment, M_0 , assuming (1) that the coseismic stress drops associated with large earthquakes are approximately constant and (2) that the stress release during an earthquake is about the same as the kinetic frictional stress during faulting. Hanks and Kanamori (1979) discuss M_w and its agreement with the M_L and M_S magnitude scales in their unsaturated ranges, while Kanamori (1983) discussed the average relationship of M_w with m_b and m_B , also in the range where these magnitudes saturate (see Fig. 3).

Traditional Amplitude-Based Magnitudes at the PTWC

Hirshorn et al. (1993) developed a short-period P-wave magnitude scale, called $pMag$, based on the average of the absolute values of the amplitudes of the first three half cycles of the initial p-waves recorded, at local distances, on short-period seismometers. The $pMag$ scale is based on the assumption that locally recorded initial P-wave amplitudes share a common decay curve shape in a given geographic area, independent of the magnitude of the earthquake, as Richter

showed was the case for S-waves in his derivation of the M_L magnitude scale for Southern California (Richter 1935). Lindh and Hirshorn incorporated $pMag$ into Carl Johnson's (1994) local p-wave associator, enabling automatic pages that contain the hypocentral parameters and the lower bound magnitude estimate provided by $pMag$, within 10 to 20 s of an earthquake's origin time.

PTWC now uses local algorithms from the stock Earthworm system (Johnson et al. 1995) to provide earthquake hypocenters and local synthetic Wood-Anderson magnitudes, M_L , for earthquakes occurring in Hawaii and the Puerto Rico/Virgin Islands Region. Depending on the density of the seismic network near the epicenter, this information is available from 20 to 60 s after earthquake origin time.

Due to the sparseness of the Caribbean network, locations from our local system are generally augmented by manual picks and stations further from the epicenter to provide additional azimuthal control for larger events. The local systems generate fairly reliable M_L magnitudes up to approximately M_6 , above which M_{wp} (Tsuboi et al. 1995, 1999; Whitmore and Sokolowski 2002) or W-phase (Kanamori and Rivera 2008)-based estimates of M_w are necessary for accurate source size estimation.

PTWC's body-wave magnitude method, $bMag$, has similarities to the intermediate period broadband body-wave m_B magnitude, as defined by the IASPEI. The IASPEI m_B (Bormann et al. 2002; Bormann and Saul 2008b) is based on Gutenberg's (1945b, c) and Gutenberg and Richter's m_B (Gutenberg and Richter 1956a, b). $bMag$ uses a 90 s window of the broadband vertical component seismogram starting 30 s prior to the arrival of the P-wave. This window is band-passed filtered between 0.3 and 5 s. The largest amplitude and its period found in the 60 s after the first P-wave arrival are used in the magnitude formula. In PTWC's implementation, the formula used is the same as Gutenberg and Richter's (Gutenberg and Richter 1956a, b) relation, adopted by IASPEI for m_B :

$$bMag = \log_{10}(A_{\max}/T_{\max}) + Q(\Delta, z)$$

where Δ is the epicentral distance ($15 \leq \Delta \leq 90^\circ$), z is the hypocentral depth (in km), A_{\max} is the maximum wave amplitude obtained from the band-pass filtered record, and T_{\max} is the period of the wave with that maximum amplitude. Gutenberg and Richter's (Gutenberg and Richter 1956b) table of $Q(\Delta, z)$ is used to provide the distance and depth corrections. The largest amplitude found in the 30 s prior to the P-wave arrival time is used as the basis for the signal-to-noise ratio. $bMag$ differs from the IASPEI m_B (Bormann et al. 2006; Bormann and Saul 2008a) in three respects:

1. $bMag$ uses the largest amplitude wave in the first 30 sec after the initial P-wave arrival time.
2. $bMag$ uses a slightly different distance range ($15 \leq \Delta \leq 90^\circ$).
3. For $bMag$, the seismogram is band-pass filtered using the band .3 to 5 s.

$bMag$ will saturate at lower magnitudes than M_S does, so it is of limited use for large earthquakes. However, $bMag$ is still useful for three main reasons:

1. Unlike M_S , $bMag$ has a correction for the depth of the event's hypocenter.
2. $bMag$ is useful for determining the magnitude of moderate earthquakes that occur after much larger earthquakes, e.g., when longer-period energy is still present in the signal from the earlier, larger event that can adversely affect magnitude methods based on those longer periods.
3. By comparison with magnitudes based on longer periods, such as M_W , the shorter-period-based $bMag$ can also provide a way to detect slow or tsunami earthquakes.

To compute M_S (as first proposed by Gutenberg 1945a and later revised by Vanek et al. 1962) at the PTWC, we first band-pass filter 14 min of the broadband velocity seismogram, from 16 to 23 s, starting 3 min before the expected arrival time of the surface waves. We then apply the following equation, similar to the IASPEI (Bormann et al. 2002; Vanek et al. 1962) formula:

$$M_S = \log_{10}(A_{\max}/T_{\max}) + 1.66 \log_{10}(\Delta) + 3.3 \\ + \text{correction}$$

The correction term is 0 for epicentral distances, Δ , greater than 16° , and $0.53-0.033\Delta$ for Δ less than 16° . This correction term allows the US TWCs to compute the M_S magnitudes from stations as close as 600 km to the epicenter, at a period of 20 s. Note that in the IASPEI implementation of M_S , because it considers a much greater period range, from 3 to 60 s for T_{\max} , there is no need for our correction term. Both the PTWC's and the IASPEI's M_S implementations are susceptible to saturation effects as the magnitude reaches the high 7's.

Although the TWCs no longer use M_S as the basis for issuing bulletins, it is still helpful in discriminating deep from shallow earthquakes and for comparing the amount of 20 s radiated energy to the amounts of radiated energy at other periods. Deep earthquakes do not excite large surface waves. Hence if $bMag > M_S$, then the hypocenter is likely to be deep.

The Mwp Method

The broadband P-wave moment magnitude, M_{wpp} , has replaced M_S as the magnitude upon which both US TWC's initial tsunami messages are based (Tsuboi et al. 1995, 1999; Whitmore et al. 2002). This is because M_{wpp} is obtained much earlier than M_S , which is based on the slower traveling surface waves, and because M_{wpp} examines much longer-period waves than the 20 s surface waves used by M_S , making it less susceptible to the saturation effects discussed above. M_{wpp} , as implemented at the PTWC, examines up to the first 120 s of the vertical component, broadband velocity seismogram, beginning at the P-wave arrival time (gray traces in Fig. 4).

The derivation of M_{wpp} assumes that we can estimate the seismic moment, M_0 , from the initial portion of the far-field P-wave observed on the vertical broadband displacement waveform, $u_z(x_r, t)$, using

$$M_0 = (4\pi\rho\alpha^3r/F^P)\text{Max}\left|\int u_z(x_r, t) dt\right|,$$

where ρ and α are, respectively, the density and P-wave velocity averaged along the propagation path, r is the epicentral distance, and F^P is the earthquake source radiation pattern (Tsuboi et al. 1995, 1999). At the PTWC, before early 2011, we followed Tsuboi et al. (1995), by approximating $\text{Max}|\int u_z(x_r, t) dt|$ by the first significant or “big” peak in the absolute value of the integrated displacement record. It is best to use velocity, $v(t)$, seismograms from broadband seismometers with flat responses out to at least 300–350 s, as there is then no need to deconvolve the instrument response from the data. Instead, we simply scale the data by a gain factor in the time domain, because we can assume that the amplitude of the instrument response function is flat over the frequency band of interest. For data from very long period broadband seismometers, such as the STS-1, Trillium 360, etc. which have flat spectral responses to velocity up to at least 300 s period, Mwp closely approximates Mw for all but the very largest and/or slowest earthquakes.

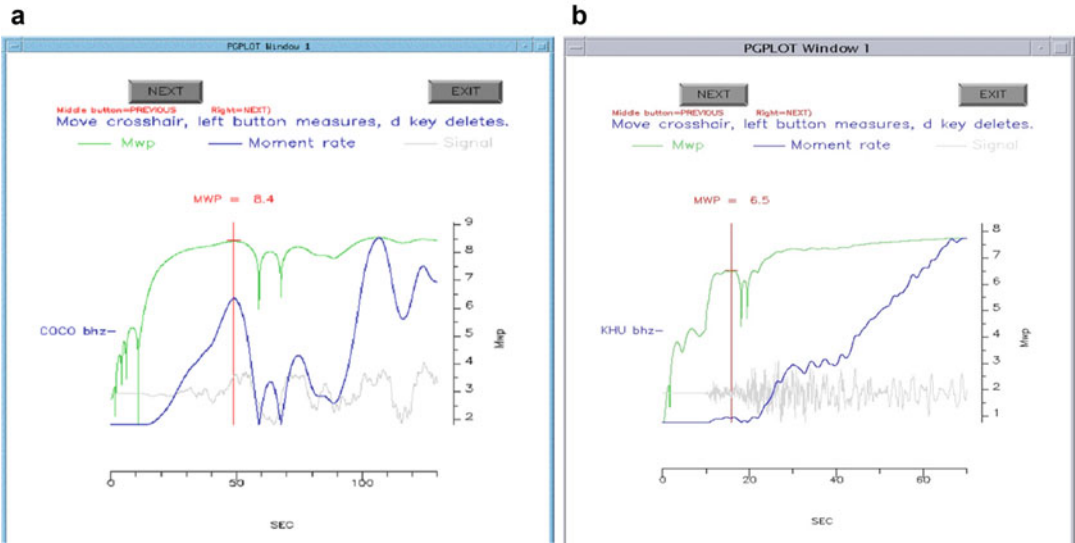
Beginning with the raw velocity seismogram, $v(t)$, we subtract the average of

300 s of $v(t)$, ending 60 s before the initial P-wave arrival time, from the entire seismogram. We then integrate twice and multiply the absolute value of each data point by $4\pi\rho\alpha^3r$ to obtain an approximation to $M_0(t)$ in N-m (the blue traces in Fig. 4). We then apply H. Kanamori's moment magnitude formula (Kanamori 1977):

$$M_W(t) = (\log_{10}M_0(t) - 9.1)/1.5$$

to $M_0(t)$, to calculate $M_{wpp}(t)$. To correct for the radiation pattern, F^P , we then add 0.2 to the average of these individual M_{wpp} values, each obtained at a different azimuth and distance from the epicenter. This is because $\int (F^P)^2 d\Omega = 4/15$ where Ω is the azimuthal angle of the observation around the epicenter; thus $F^P \propto \sqrt{4/15} = 0.52$. Therefore, we correct the averaged M_0 by adding 0.2 to M_{wpp} . Finally, we apply the Whitmore et al. (2002) magnitude-dependent correction $M_{wpp} = (M_{wpp} - 1.03)/0.843$ to get a final value for M_{wpp} (the green traces in Fig. 4).

Figure 5 compares our final M_{wpp} values resulting from this procedure (using vertical component velocity data from STS1 and/or KS54000 broadband seismometers for 291 earthquakes of Mw 4.5 to 9.2, occurring between 2002 and 2014) with (GCMT) moment magnitude M_W estimates. For some earthquakes, such as the complex M_W 8.4 (GCMT) Peru event of June 23, 2001, or the great M_W 9.2 (Ammon et al. 2005; Park et al. 2005; Stein and Okal 2007a, b) Sumatra earthquake of December 26, 2004, M_{wpp} (7.4 and 8.1, respectively) will underestimate M_W , when the first moment release is not the largest and/or significant moment release follows the initial moment release by a sufficiently long time. The 2001 Peru Mw 8.4 earthquake began with an initial rupture of moment magnitude approximately 7.4, followed almost 60 s later by a much larger earthquake, of moment magnitude just under GCMT Mw 8.4. In contrast, the PTWC's final estimate of M_{wpp} 8.4 for the M_W 8.6 (Centroid Moment Tensor 2008) Nias event of March 28, 2005, was acceptable, as it was for the M_W 8.1 Chile earthquake of April 1, 2014 (Bryant 2001), and for other earthquakes in the M_W 8.0 to 8.4 range. M_{wpp} thus enables Regional tsunami



Earthquake Source Parameters, Rapid Estimates for Tsunami Forecasts and Warnings, Fig. 4 (a) Is the first 2 min of the broadband vertical velocity seismogram beginning with the p-wave arrival (gray) recorded by the GSN USGS/IRIS broadband station COCO, on Cocos Island, ~15 degrees south of the epicenter of the M_w 9.2 Sumatra earthquake of Dec. 26, 2004. Note that this portion of the broadband velocity seismogram is not clipped.

This instrument, a KS54000, has a flat frequency response to velocity to a period of about 350 s. The blue trace is the integrated displacement record (doubly integrated velocity) $\sim Mo(t)$, and the green trace, $M_{wp}(t)$, is M_{wp} as a function of time. (b) Shows these results at KHU, 77 km from the epicenter of the Mw6.7 (GCMT) Kiholo Bay Hawaii earthquake of October 16, 2006

warnings (for coastal populations within 1000 km of the epicenter) within 3–5 min of earthquake origin time, as the threshold for a regional warning is Mw 7.6.

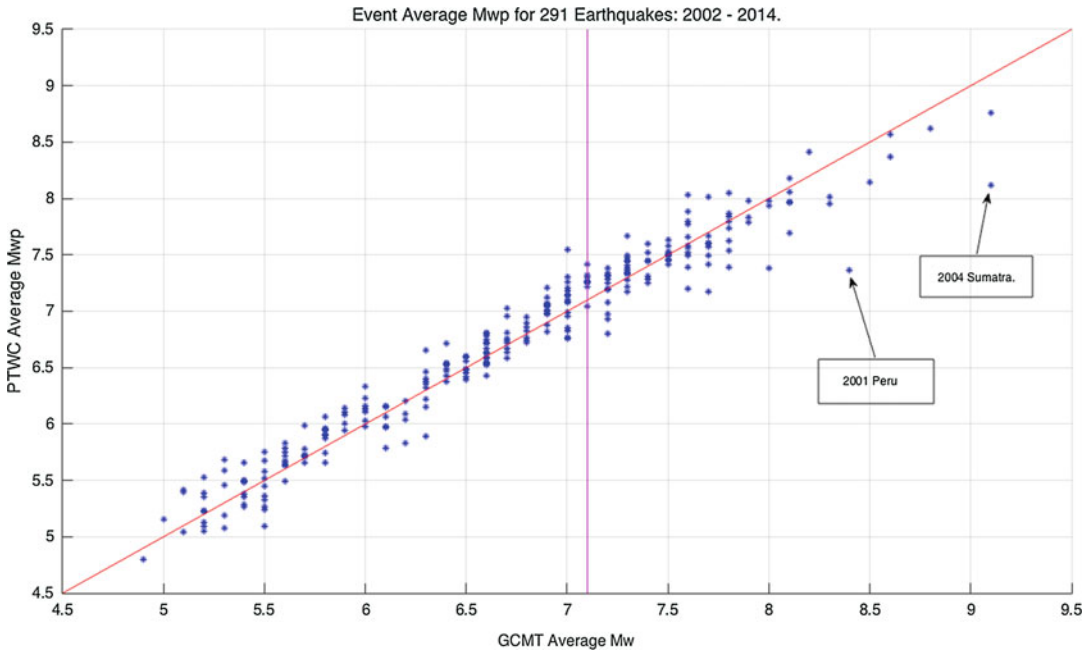
At the PTWC, beginning in early 2011, we have automated the M_{wp} method in the following way:

1. Compute a signal-to-noise ratio by examining 60 s of trace prior to, and after, the P-wave arrival time. Both sections are band-pass filtered between .3 and 5 Hz and the rms mean computed for each. The ratio of these two means yields the signal-to-noise ratio. If the ratio is above 5.0, the auto-Mwp proceeds.
2. Compute the average of the unfiltered noise over a 300 s interval, ending 60 s prior to the P-wave arrival time. This provides a baseline correction for the integration.
3. Doubly integrate the first 120 s of the unfiltered seismogram (minus the noise average determined in step 2), beginning at the P-wave

- arrival time up to the S-wave arrival or 120 s, whichever comes first, to compute $M_0(t)$.
4. Examine the curve for peaks. This is called the monotonicity check. If there are no clear peaks, then this station may be rejected for auto-Mwp; however it remains available for manual analysis.
5. Recursively smooth the moment(t) curve until three main peaks are left. The algorithm then uses the location of these peaks as a guide to search for the peaks on the original, unsmoothed moment rate curve. This allows us to apply the Tsuboi method (Tsuboi et al. 1999) to the first two peaks of a smoother waveform, so that this can be done automatically, in real time.

PTWC scientists have also designed a GUI that allows the duty scientists to quickly evaluate the quality of each of these automatically generated M_{wp} measurements.

The GUI (Fig. 6) shows the auto-Mwp results available for review at 6 min after origin time, for



Earthquake Source Parameters, Rapid Estimates for Tsunami Forecasts and Warnings, Fig. 5 A scatter plot of event average PTWC M_{wp} values against GCMT M_w for 291 earthquakes in the M_w 4.5–9.2 range occurring between 1992 and April of 2014. These M_{wp} event averages were derived only from very broadband vertical

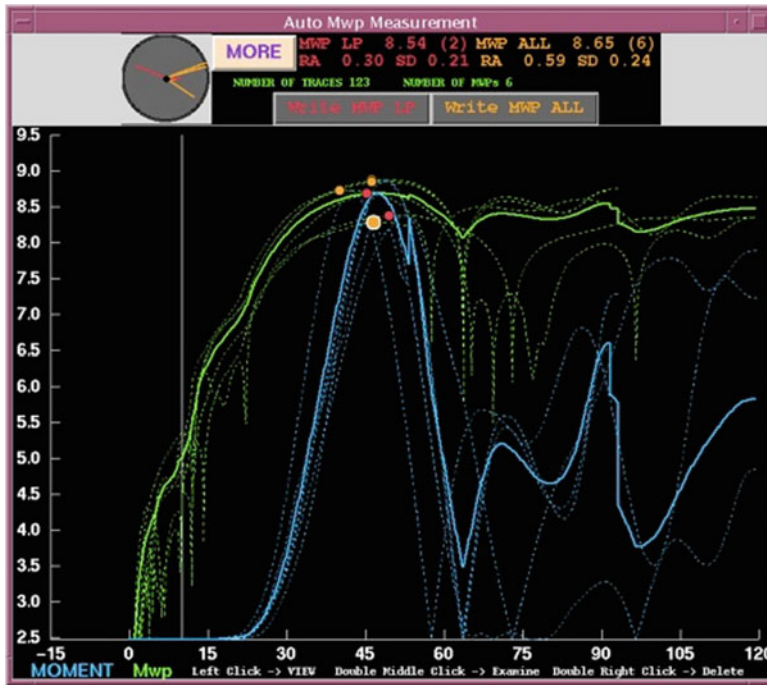
seismograms (STS1 and KS5400 seismometers only). The red line represents $M_{wp} = M_w$, and the vertical magenta line defines the NOAA/NWS Tsunami Warning Center’s (TWC’s) threshold for issuing a local tsunami warning for coastal populations within 300 km of the event’s epicenter

the closest six stations to the first of two great earthquakes offshore Sumatra that occurred on April 11, 2012. Note that the resulting M_{wp} value of 8.65 agrees well with the GCMT M_w of 8.6. At the top of the GUI are two summaries, showing the mean M_{wp} based on long-period instruments (red), based on all instruments (orange), and a plot showing the azimuthal distribution of stations, the number of traces processed, and the total number of M_{wp} measurements obtained. There are also three buttons, two of which allow the duty scientist to select the M_{wp} values based on just the long-period instruments or those based on all instruments, and another button “MORE” which will display additional M_{wp} measurements. Auto- M_{wp} will stop updating M_{wp} in its real-time mode after computing 40 measurements. This is generally many more observations than needed for an accurate estimate of M_w .

The plot (of Fig. 6) shows all of the $M_0(t)$ curves obtained (dashed-blue), the $M_{wp}(t)$ curves (dashed-green), and the stacked $M_0(t)$ and

$M_{wp}(t)$ curves, thick blue and green curves, respectively. The dots show where the auto- M_{wp} algorithm has computed the M_{wp} for the various stations. As can be seen in Fig. 6, the stacked $M_0(t)$ curve has one main peak that is populated by six measurements. The solid curves result from stacking the results of all six instruments. The stacked $M_{wp}(t)$ curve (green) is obtained from the stacked $M_0(t)$ curve (blue).

The PTWC also calculates M_{wp} from locally recorded P-waves to estimate M_w for large ($> \sim M_w 5$) local earthquakes, occurring in the Hawaiian Islands (Hirshorn 2004, 2007), Puerto Rico, the Virgin Islands, and California. Because M_{wp} is based on the far-field approximation to the (vertical) P-wave displacement due to a double couple point source (Tsuboi et al. 1995), we should only very carefully apply M_{wp} to data obtained in the near field, at distances of less than a few wavelengths of the fault. At about 5 degrees epicentral distance, the point source approximation appears to be valid up to about GCMT M_w 7.5–8 (see Fig. 7). Figure 7 is a



Earthquake Source Parameters, Rapid Estimates for Tsunami Forecasts and Warnings, Fig. 6 The PTWC’s AutoMap graphical user interface (GUI) showing the $M_0(t)$ curves (dashed-blue), the $M_{wp}(t)$ curves (dashed-green), and the stacked $M_0(t)$ and $M_{wp}(t)$ curves, thick blue and green curves, respectively, for a single earthquake. The

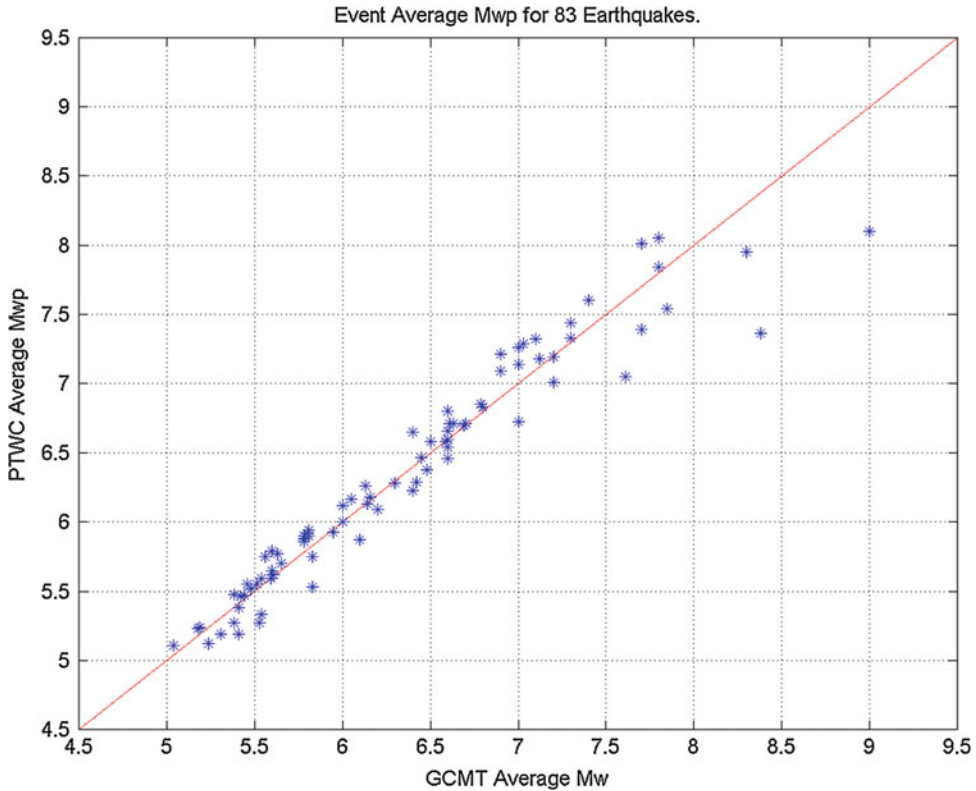
dots show where the auto- M_{wp} algorithm has computed the M_{wp} for the various stations. The stacked $M_0(t)$ curve has one main peak that is populated by six measurements. The solid curves result from stacking the results of all six instruments. The stacked $M_{wp}(t)$ curve (green) is obtained from the stacked $M_0(t)$ curve (blue)

plot of M_{wp} values calculated from locally recorded P-waves, up to 5 degrees epicentral distance, against the GCMT M_W values for the same events. For example, PTWC scientists calculated a value of Mwp 6.5 for the GCMT M_W 6.7 Kiholo Bay, Hawaii, earthquake within 3 min of the initiation of rupture at its hypocenter (Hirshorn 2007). Based on data provided later to the PTWC for the 2011 GCMT 9.1 Off Tohoku earthquake, accurate M_{wp} determinations of 9.3, 9.3, and 9.1, were obtained at 10.9, 12.4, and 14.9 degrees epicentral distance, respectively (Hirshorn et al. 2013). M_{wp} estimates from these 18 STS-1 broad band velocity records at 2.2–14.9 degrees epicentral distance, all exceeded the PTWC’s threshold for a Tsunami Threat Message for coastal populations within 1000 km of the earthquake.

The Mantle Magnitude (M_m) Method

Emile Okal and J. Talandier developed the M_M method in 1989 (Okal and Talandier 1989). The mantle magnitude is related to the moment magnitude via the simple expression $M_W = M_m / 1.5 + 2.6$. This work was inspired by the need to develop a magnitude method for tsunami warning centers that would not suffer the saturation problem that M_S suffers (Okal 1992a). Not only may M_S saturate as M_W becomes large (>8), but slow earthquakes can also cause M_S to be seriously deficient and $bMag$ even more so. Severely underestimating the magnitude of an earthquake can lead to a failure to warn. PTWC’s implementation of the M_m method is based on analyzing Rayleigh waves obtained on vertical component seismograms.

M_m , being based on slow traveling long-period surface waves, is available too late to be used in the decision process for issuing an initial bulletin.



Earthquake Source Parameters, Rapid Estimates for Tsunami Forecasts and Warnings, Fig. 7 A scatter plot of 83 Mwp event averages obtained from observations

within 5 degrees epicentral distance from their respective epicenters, plotted against the GCMT event Mw for the same earthquakes

Notwithstanding, it does provide a useful check on the magnitude obtained from the M_{wp} method, and if there is a discrepancy between M_{wp} and $M_W(M_m)$ on the order of 2–3 tenths or more in the 7^+ magnitude range, then the duty scientist may instead use the results of the M_m method in subsequent bulletins. The M_m method overcomes the limitation of saturation because it is a variable period magnitude. Multiple values of M_m are routinely computed for a number of fixed periods ranging from 50 to 270 s for each station. Because M_m may saturate at smaller periods for great earthquakes while remaining unsaturated at longer periods, Okal and Talandier's (1989) procedure was to choose the largest M_m , thus mitigating the effects of saturation.

M_m is more complicated than the other magnitude methods described here as it uses frequency-domain deconvolution. This can cause problems due to deconvolution noise at low magnitudes,

where the amplification of noise by the deconvolution process at long periods may result in spurious magnitudes. Thus M_m works best with very long-period broadband seismometers. While STS-2 seismometers tend to do well, the shorter-period broadband seismometers tend to behave poorly at the longest periods (Weinstein and Okal 2005). Using the maximum M_m obtained for each station proved to be suboptimal due to the heterogeneous distribution of instruments coupled with the total automation of the procedure at the PTWC. Weinstein and Okal (2005) devised a sampling method that alleviates most of these difficulties in PTWC's implementation of M_m .

The December 2004 Sumatra earthquake showed that for earthquakes with an unusually long source duration (in this case ~ 600 s) (Ishii et al. 2005; Kanamori 2006), even M_m calculated using 270 s waves will saturate. Hence PTWC's M_m implementation will now automatically

extend the period range to 410 s when the magnitude exceeds 8.0. At 410 s $M_W(M_m)$ is 8.9 (Weinstein and Okal 2005) for the GCMT M_W 9.2 December 2004 Sumatra earthquake, still deficient, but a marked improvement over the moment magnitude 8.5 obtained by PTWC and 8.2 obtained by the USGS (NEIC Fast Moment Tensor) on Dec. 26, 2004. M_m normally uses a 660 s window of the surface wave train, but when M_m exceeds 8.0, it expands this window to 910 s. Given the mix of instruments and their distribution used by the PTWC and the effects of broadband deconvolution noise, Weinstein and Okal (2005) found that the M_m method was usually not useful for earthquakes smaller than M_W 6.0. Since publication of that study, PTWC has made some refinements to the M_m calculation. PTWC computes the “noise floor,” i.e., the M_m spectra using data obtained before the earthquake origin time, for each seismic station. M_m values obtained for the earthquake are compared to those obtained from the pre-event noise. If the seismic moment obtained at any period is less than a factor of 10 above the seismic moment obtained from the pre-event noise, the value for M_m at that period is rejected. For smaller earthquakes with $M_w < 6.0$, this typically means that values of M_m at longer periods get rejected. With this technique, PTWC routinely obtains credible magnitude estimates based on mantle waves for earthquakes with magnitudes as small as 5.5 and sometimes even smaller depending on the noise floor. The same technique also eliminates measurements that may be contaminated by mantle waves generated by very recent earthquakes.

Figure 8 compares $M_W(M_m)$ values obtained for more than 200 earthquakes with the respective GCMT M_W values for the same events. PTWC’s implementation of M_m tends to overestimate M_W by 0~0.15 magnitude units for $M_m < 7.0$.

The W-Phase Method

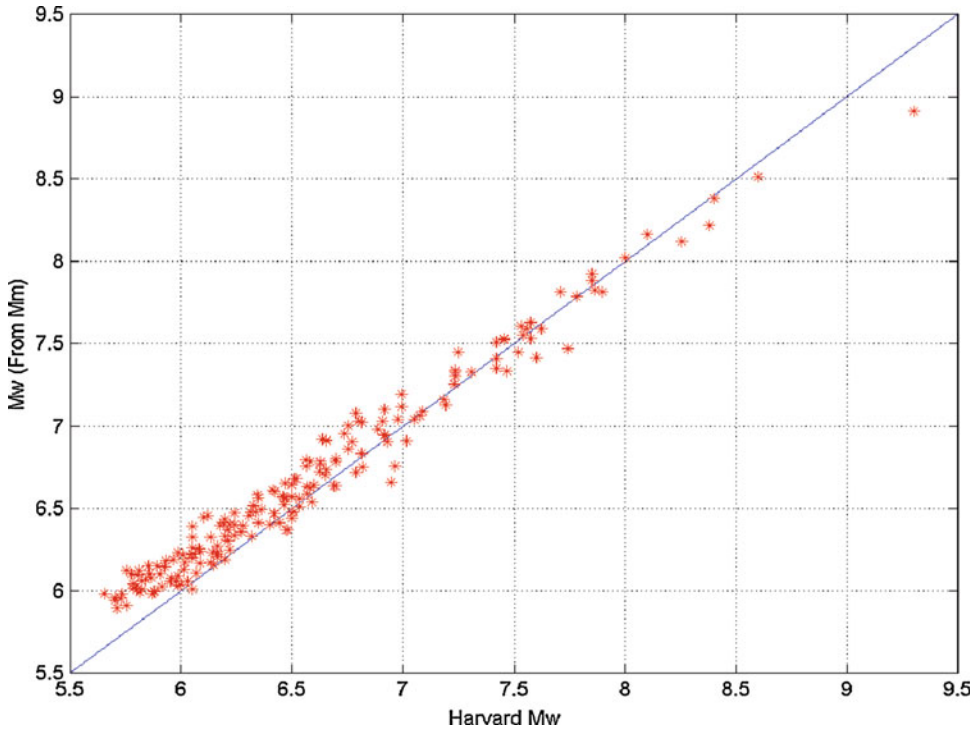
H. Kanamori first identified the W-phase on displacement seismograms generated by the 1992 Nicaragua tsunami earthquake (Kanamori 1993). This earthquake was deficient in high-frequency radiation but rich in long-period energy (see Fig. 9).

When the periods of phases such as P, PP, S, SS, SP, etc. approach or exceed the travel time differences between them, the phases will interfere with each other. At these long periods, the result of this interference is itself a distinct phase now called the W-phase (Kanamori 1993).

The name W-phase was chosen because this phase is analogous to the “whispering gallery” mode of wave propagation found in acoustics or optics (Kanamori 1993). An example of the optical whispering gallery mode is light trapped inside a raindrop. The raindrop acts a like an optical fiber loop with the light strongly concentrated near the surface of the drop. P. Cummins showed that the W-phase could also be modeled as the complete elastic wave field (near field + far field) (Cummins 1997).

In the context of normal mode theory, the W-phase can be interpreted as the superposition of the fundamental mode and the first, second, and third overtones of spheroidal modes at long periods (Kanamori and Rivera 2008). The group velocity of the W-phase varies from 4.5 km/s to 9.0 km/s over a period range from 100 to 1000 s. Like mantle waves, most of the energy in the W-phase propagates within the mantle, so that the propagation of the W-phase is little affected by the complications of structural heterogeneities such as continents and oceans.

Because of the W-phase’s very long-period character, magnitude estimates based on it should not saturate, even for truly great earthquakes. H. Kanamori and L. Rivera demonstrated this for the great M_W 9.2 Sumatra earthquake of 2004, with a source duration of ~600 s (Kanamori and Rivera 2008). The true magnitude of the Sumatra earthquake of 2004 was not known until 2005, when enough seismic data were recorded (weeks) for stacking, to allow the amplitudes of the Earth’s free oscillations to be accurately measured (Park et al. 2005). H. Kanamori and L. Rivera’s W-phase method (Kanamori and Rivera 2008) now provides magnitudes and centroid moment tensors for great earthquakes to PTWC duty scientists, within about 25 min after the initiation of rupture at the hypocenter. For the 2011 M_w 9.0 Tohoku, Japan, earthquake, PTWC’s W-phase implementation yielded an M_w of 9.0 when



Earthquake Source Parameters, Rapid Estimates for Tsunami Forecasts and Warnings, Fig. 8 Scatter plot of $M_w(M_m)$ vs. GCMT M_w for over 200 earthquakes

provided with the correct depth (Duputel et al. 2011) (Figs. 10 and 11).

Luis Rivera, Zacharie Duputel, and PTWC scientists implemented the W-phase method at the PTWC in late 2010. W-phase processing begins when the PTWC issues an observatory message. If the earthquake's magnitude is ≥ 5.8 , then the software will compute a W-phase CMT. W-phase results are sent to the duty scientists if the magnitude in the observatory message is 6.8 or larger. The W-phase CMT computations for earthquakes in the M_W 5.8 to 6.7 range enable research and debugging, but are not used for tsunami warning purposes.

The GCMT M_W 9.1 Tohoku earthquake of March 10, 2011, provided an excellent test of the PTWC's W-phase processing. Figure 11 is a table showing the evolution of the W-phase CMT with time (Duputel et al. 2011). The PTWC obtained an initial W-phase CMT 22 min after the earthquake's origin time. Because our initial depth determination was too deep, the magnitude was

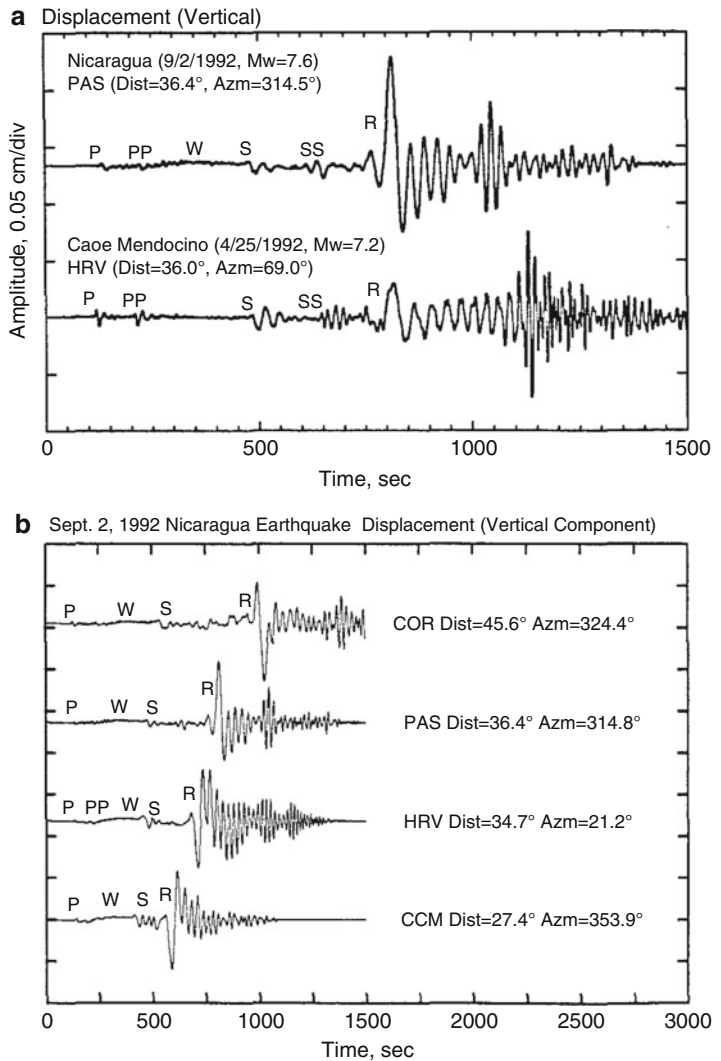
underestimated. When manually re-triggered with a better hypocentral depth, 44 min after origin time, PTWC obtained M_W 9.0 and a CMT consistent with the USGS and GCMT M_w values (Hayes et al. 2011).

Tsunami Earthquakes

Tsunami earthquakes are so-called because they generate tsunamis that are more destructive than expected given their magnitude. Classic examples include the Nicaragua 1992 (Fig. 9) and Java 2006 earthquakes. Tsunami earthquakes present a challenge to tsunami warning systems because they generate much less ground shaking than expected given their size. Hence populations near the earthquake, which otherwise might be alerted by strong ground shaking, may not self-evacuate if they are not alarmed by the ground shaking. Tsunami or "slow" earthquakes also present a challenge to warning centers because their unique rupture characteristics affect magnitude determinations. These two characteristics, i.e., difficulty in

Earthquake Source Parameters, Rapid Estimates for Tsunami Forecasts and Warnings,

Fig. 9 W-phase observed for the September 2, 1992, Nicaragua earthquake. Figure 10a compares the Nicaragua earthquake with a Cape Mendocino earthquake. Figure 10b shows the seismograms of the Nicaragua earthquake recorded at stations COR, PAS, HRV, and CCM. All the seismograms show displacement computed from the original broadband seismograms. (Figure 1 from Kanamori 1993)

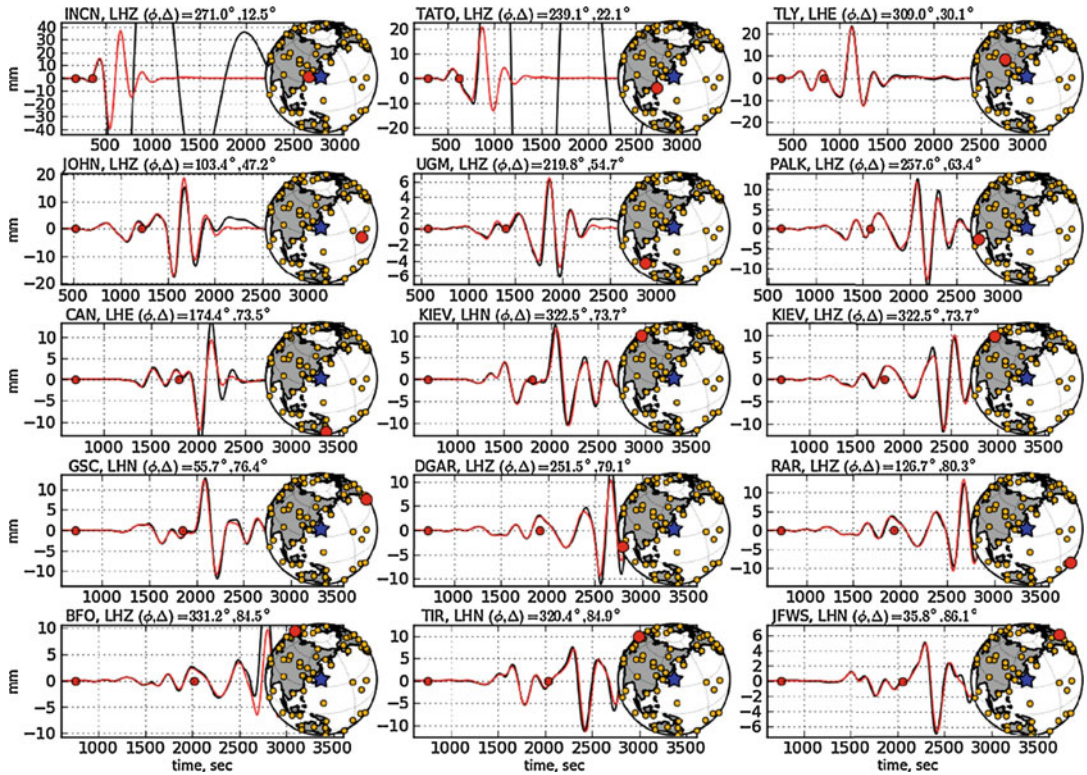


determining correct magnitude and generating larger tsunamis than expected (even with the correct magnitude), contribute to the possibility of under warning coastal populations of a destructive tsunami. Fortunately, there are methods to alert duty scientists to the occurrence of tsunami earthquakes.

One way in which the occurrence of a tsunami earthquake may be detected is if the bMag and/or MS are significantly smaller than M_{wp} obtained from the longer-period P-waves or longer-period mantle waves. Figure 12 shows this clearly for short-period \hat{m}_b (Gutenberg and Richter 1956b) Vrs. M_w . Note the population of four tsunami earthquakes that fall well off the trend. As can be

determined from Fig. 12, the body-wave magnitude for July 2006 Java earthquake was deficient by nearly 1.5 magnitude units.

As mentioned earlier, a fundamental characteristic of a tsunami earthquake is the slowness of the rupture speed. Newman and Okal (1998) showed that the log ratio of the radiated energy E_R (Boatwright and Choy 1986; Boatwright et al. 2002), to the seismic moment M_0 , $\text{Log}_{10}(E_R/M_0)$ (also denoted by theta or “ θ ”) is anomalously small for tsunami earthquakes. A number of factors can affect this ratio such as rupture velocity, stress drop/apparent stress, fault plane geometry, maximum strain at rupturing, and directivity (bilateral vs. unilateral rupture). However,



Earthquake Source Parameters, Rapid Estimates for Tsunami Forecasts and Warnings, Fig. 10 Examples of observed waveforms (black lines) and the corresponding synthetics (red lines) computed from the W-phase solution for the GCMT Mw 9.1 Tohoku earthquake. The station azimuth (ϕ) and epicentral distance (Δ) are indicated as

well as W-phase time window, bounded by red dots. W-phase and later arrivals are often very well predicted by the solution. For some channels like INCN-LHZ or TATO-LHZ, the surface waves are affected by instrument problems, though the earlier-arriving W-phase signal is not affected. (Figure 3 from Duputel et al. 2011)

for shallow thrust, low stress drop subduction zone earthquakes, unusually slow rupture velocity may have the largest influence on the value of θ .

Newman and Okal (1998) showed that for tsunami quakes, the value of θ is usually -6.0 or less. For an earthquake with a unilateral rupture and nominal speed (~ 3 km/s), theory suggests that θ is -4.9 (Geller and Kanamori 1977; Scholz 1982; Vassiliou and Kanamori 1982). Weinstein and Okal (2005) extended the original dataset of Newman and Okal (1998) by including an additional 118 earthquakes. The mean value of all θ values is approximately -5.1 . However, when averaged by event, the distribution of θ 's peaks precisely at -4.9 , in accordance with theoretical expectations. Given the standard deviation of 0.39 for all θ 's (for the 118 earthquakes), Weinstein and Okal (2005) found that values of θ around -6.0 or

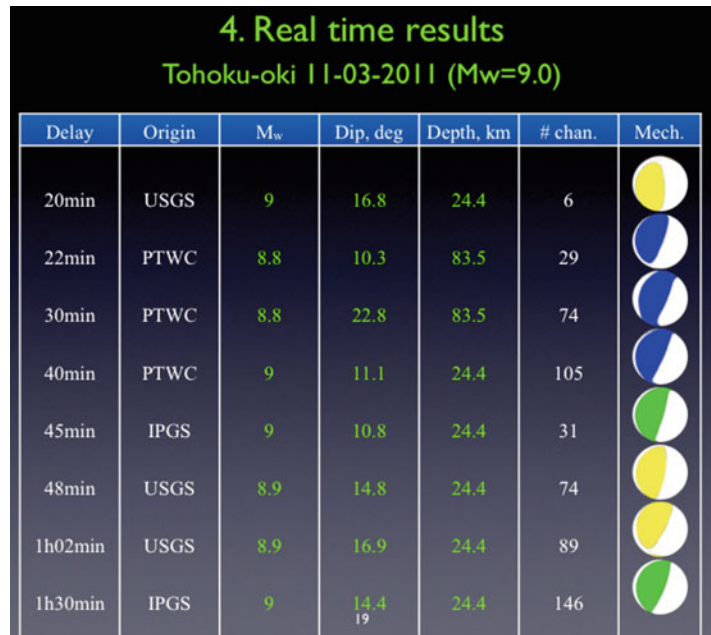
below are more than 2σ off of the mean and hence clearly anomalous.

The PTWC uses broadband vertical component seismograms, obtained in the distance interval $5^\circ \leq \Delta \leq 90^\circ$, to compute θ . Originally, the closest distance was 25° . However, this can be made as close as 5° using new corrections (Ebeling et al. 2012). A window of 75 s is used starting approximately 5 s before the P-wave arrival to insure that the first arrivals are not missed by the integration. This window is deconvolved with the instrument response, and the radiated energy contained between 1 and 2 Hz is computed.

In general, it is thought that anomalously slow rupture speed is due to either low-rigidity sediments in the fault and/or faulting through an accretionary prism (Bilek and Lay 1999; Bilek

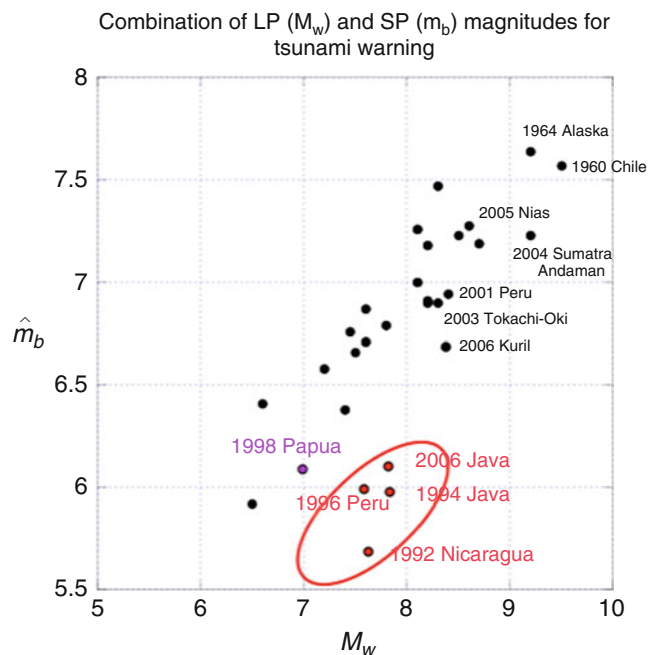
Earthquake Source Parameters, Rapid Estimates for Tsunami Forecasts and Warnings,

Fig. 11 Real-time W-phase results from the USGS and the PTWC from Duputel et al. (2011)



Earthquake Source Parameters, Rapid Estimates for Tsunami Forecasts and Warnings,

Fig. 12 Comparison between short-period \hat{m}_b (Gutenberg and Richter 1956b) and M_w for earthquakes with $M_w > 6$. Note the cluster of red dots representing tsunami earthquakes. This illustrates the diagnostic potential of short-period/long-period magnitude ratios to identify unusually slow earthquakes with high tsunami potential (This is Hiroo Kanamori’s figure from his talk at the PTWC in April of 2007)



et al. 2004; Fukao 1979; Kanamori 1972; Kanamori and Kikuchi 1993; Satake 1994). In either case, the small shear rigidity associated with weak materials retards the rupture speed. As to why “slow” earthquakes produce more destructive than expected tsunamis, one can look

at the well-known relation for moment magnitude:

$$M_0 = \mu A d$$

where μ is the shear modulus, A is the fault plane area, and d is the average slip over the fault plane. Thus, for two earthquakes with the same seismic moment (M_0), and fault area (A), lowering μ (i.e., decreasing the rupture propagation speed) requires increasing the slip (d) to keep the M_0 (and M_w) the same. Hence a slow rupturing, Tsunami earthquake produces larger-than-expected slip and therefore tsunami, based on seismic moment.

One problem with θ is that it can be misleading and occasionally yield false indications of rupture slowness. This was made apparent by the Peru earthquake of June 23, 2001. This earthquake began with an initial event that had a moment magnitude of approximately 7.4, followed almost 60 s later by a much larger event, which had a moment magnitude of almost 8.4. (Bilek and Ruff 2002; Giovanni et al. 2002; Kikuchi and Yamanaka 2001). Due to the 60 s delay, the θ computation used mainly P-wave coda from the first shock and little if any energy from the main shock. As a result, the PTWC initially obtained a θ of -6.1 , using a moment based on Mm, making this earthquake appear very slow indeed. However, this result is spurious and was due to the complexity of the earthquake itself and not to actual slowness of the rupture.

Weinstein and Okal (2005) found that by sliding the window over which θ is computed forward in time, θ would increase as the θ window overlapped with the occurrence of the main event of the Peru 2001 earthquake. Indeed, for a window offset of 70 s, θ increases to -5.6 , which is a strong trend to slowness, but not a slow or tsunami quake. This was further borne out by the size of the tsunami, which while detected on sea-level instruments around the Pacific (more than 2 m peak to trough in Chile) was not destructive outside of Peru.

Weinstein and Okal (2005) explored the windowing technique and found that it was a more comprehensive method than the single determination of θ (zero offset). Computing theta in a succession of windows separated in time by 10 s (each window spanning 70 s) up to 100 s post P-wave arrival yields a better method of detecting slowness; see Fig. 13. What Weinstein and Okal (2005) found is that for true tsunami earthquakes, the variation of θ with offset time was small,

generally no more than 0.1 log units over the entire 100 s. It is this flat trend that is probably the best discriminant for tsunami earthquakes.

In effect, the curve resulting from the window-offset technique gives an indication of the source duration of the earthquake. Gigantic earthquakes have long source durations, and slow earthquakes have anomalously long source durations for their seismic moment; see Fig. 13. Therefore θ can be viewed as a measurement of how anomalous the source duration is in terms of whether the earthquake is anomalously slow or simply anomalously large. It turns out that in the case of the Sumatra earthquake of December 2004, θ has little variation, even when the integration window is increased to 200 s and the offset carried out to 300 s. The magnitude of θ based on PTWC's Mw (Mm) of 8.5 was ~ -5.6 , a trend to slowness, but not slow. Using the Mw based on normal mode studies, θ is ~ -6.1 (with a 200 s integration window!), and discussion continues to the current day as to whether or not the Sumatra earthquake of 2004 was slow and simply had aspects of a tsunami earthquake or none at all (Ammon et al. 2005; Global Centroid Moment Tensor (GCMT); Krüger and Ohrnberger 2005; Lay et al. 2005; Seno and Hirata 2007).

Real-Time Tsunami Forecasting

Historically, tsunami warning centers (TWCs) issue tsunami warnings based on the initial earthquake magnitude (based on historical events) and tsunami travel times. Pre-computed databases of tsunami scenarios can also be used to provide a quick estimate of a possible tsunami threat (Gica et al. 2008; Kamigaichi 2009; Kowalik and Whitmore 1991; Tatehata 1997). The principle limitation of the database approach is that it cannot exhaust all possible earthquake source parameters and locations. Due to advanced computer technology and the development of rapid real-time source inversion methods such as the W-phase method (Duputel et al. 2011, 2012; Hayes et al. 2009; Kanamori and Rivera 2008), real-time tsunami forecasting, using real-time earthquake parameters and other contemporaneous observations (e.g., GPS and water level observations), has become a reality. W-phase centroid moment tensors (CMT) obtained during events

Earthquake Source Parameters, Rapid Estimates for Tsunami Forecasts and Warnings, Fig. 13 The variation of Θ with offset for (a) a “normal” earthquake, (b) a “slow earthquake” (Java, 2006), and (c) a complex earthquake (Peru, 2008), respectively. In these plots Θ is demeaned (the mean is found on the bottom right of the plot in black), and the number next to the dots indicates how many stations were used in computing that value. These plots are taken from PTWC’s operational software



have been used in a real-time forecast model at PTWC (Duputel et al. 2011; Fryer et al. 2010; Wang et al. 2012) since 2011. Offshore GPS buoy data can be used to constrain the tsunami sources in real time (Yasuda and Mase 2013). Land-based GPS data can also be used to constrain the tsunami source in a real-time model (Hoechner et al. 2013).

PTWC started experimenting with a real-time tsunami forecasting model RIFT in 2009. Starting in 2014, RIFT became the basis of the forecast products issued with PTWC tsunami threat messages (Wang et al. 2009). The typical work cycle is the following:

- (1) As soon as the earthquake has been located and the magnitude determined, the model is run for regions near the epicenter (within several hours of tsunami arrival time), using the real-time earthquake location and magnitude with default focal mechanisms. The default focal mechanism is based on the type of plate boundary the earthquake is closest

to. To be conservative, a pure thrust mechanism along subduction zones can be assumed, and the strike used is the strike of the trench axis. Alternatively, a normal faulting or strike-slip faulting focal mechanism can also be used if the epicenter is near a divergent plate boundary or a strike-slip plate boundary, respectively. The model results for the near field can be obtained in a few seconds.

- (2) Once the W-phase centroid moment tensor becomes available (typically within 20–30 min of the earthquake origin time), the model is run again to update the forecast. A larger model domain (e.g., the entire Pacific basin) can be used for large earthquakes.
- (3) The model forecast is compared with water level observations to confirm or refine the forecast.

The RIFT model is based on the finite difference discretization of the linear shallow water equations:

$$u_t = -g\nabla\eta,$$

$$\eta_t + \nabla \cdot (uh) = 0,$$

where $u = (u,v)$ is the vertically averaged horizontal velocity, η the sea surface elevation, h the ocean depth at rest, and ∇ the horizontal gradient operator. The model is discretized in spherical coordinates with a leapfrog time differencing scheme on the Arakawa C-grid (Arakawa and Lamb 1977). The numerical scheme is similar to that of Imamura except that the staggered leapfrog time differencing scheme is used (Imamura 1996).

The initial condition is based on the static seafloor deformation formula of Okada (1985) for a rectangular rupture zone with a uniform slip. The assumed rupture size is a continuous function of earthquake magnitude (Henry and Das 2001; Wells and Coppersmith 1994). The coastal wave amplitude is based on the Green's law (Lamb 1932),

$$a_c = a_o(h_o/h_c)^{1/4}$$

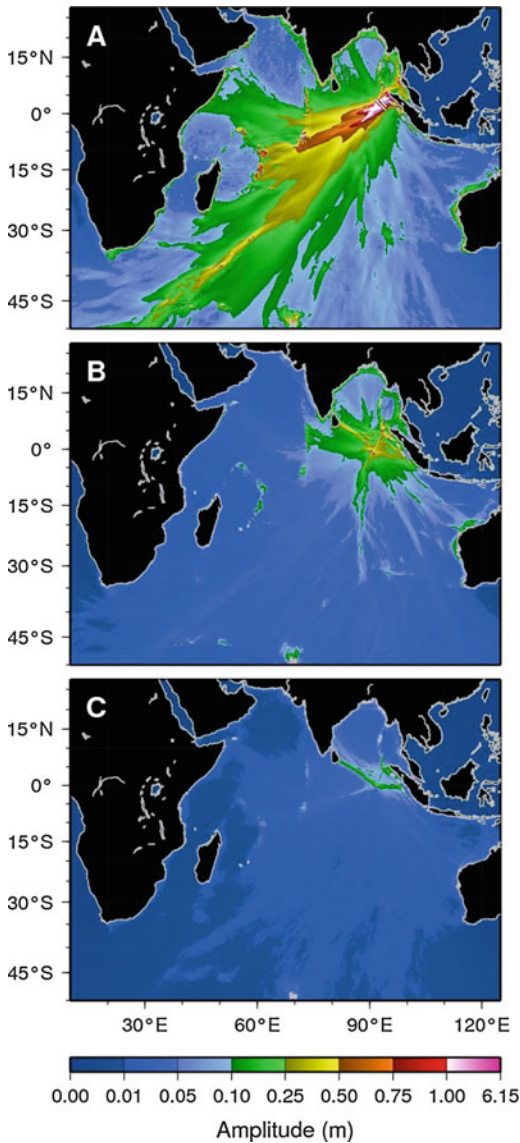
where a_c and a_o are wave amplitudes at a coastal point and an corresponding offshore point. h_c and h_o are water depths at the coastal point and the offshore point, respectively. The offshore point is chosen such that the water depth is greater than a threshold value (typically 1000 m at 4-arc-min resolution or smaller depth for finer resolution). The wave amplitude is defined as half of the wave height, which is the difference between the trough and crest of the wave. We should point out that the Green's law coastal forecast is most applicable for coastlines that are directly exposed to the open ocean. The Green's law is not applicable for locations that are not exposed to the open ocean directly (such as harbors well hidden from the open ocean, fjords, and rivers). Nevertheless, the Green's law forecast should provide a quick order of magnitude estimate of general tsunami threat for tsunami warning purposes.

The bathymetry used by RIFT is based on the 30-arc-sec resolution GEBCO data (Becker et al. 2009). The operator of the model can choose 1 of 40 predefined ocean basins or use a basin

determined on the fly by a tsunami travel time software (Wessel 2009; Wessel and Smith 1991). This is the default basin setting. A forecast for this default model domain can be obtained in ~ 10 s at 4-arc-min resolution on a 12-CPU Linux server. A 30-h forecast for the entire Pacific basin at 4-arc-min resolution can be obtained in 7 min. For smaller earthquakes (magnitudes < 7.5) or earthquakes that only have a regional impact (e.g., a local earthquake in Hawaii), a smaller domain and higher resolution can be used.

Timeliness is essential for tsunami warning. The linearization of the shallow water equations and the use of the Green's law in the RIFT model allow for rapid forecast of tsunami threats. The RIFT model was run for most of the events since 2009 for which measurable tsunamis were recorded. The results are encouraging. As an example, we discuss the April 11, 2012, magnitude 8.6 earthquake off the northern Sumatra coast and the ensuing tsunami (Wang et al. 2012). Based on an initial earthquake magnitude of 8.7, the PTWC issued an Indian Ocean basin-wide tsunami watch. The governments of India, Indonesia, Sri Lanka, Thailand, and the Maldives also issued Tsunami warnings.

Figure 14 shows three RIFT forecast results obtained during the event. The top panel (Fig. 14a) shows the maximum wave amplitude for a default shallow thrust mechanism (based on PTWC's initial earthquake M_{wp} magnitude of 8.66). The forecast was obtained 14 min after the earthquake origin. It forecasts a tsunami posing a significant threat to some Indian Ocean countries, with a maximum coastal wave amplitude using Green's law of 9 m. The middle panel (Fig. 14b) shows the maximum wave amplitude from the RIFT model using the PTWC's W-phase CMT solution ($M_w = 8.78$) obtained 39 min after the earthquake origin time. Although the earthquake magnitude obtained from this CMT was greater than the initial estimate based on the M_{wp} method, the tsunami wave amplitudes were reduced substantially. The maximum coastal wave amplitude was only 2.4 m near the epicenter, and only a handful of coastal locations experienced wave amplitudes over 1 m. This reduced tsunami amplitude is due to the earthquake's strike-slip focal



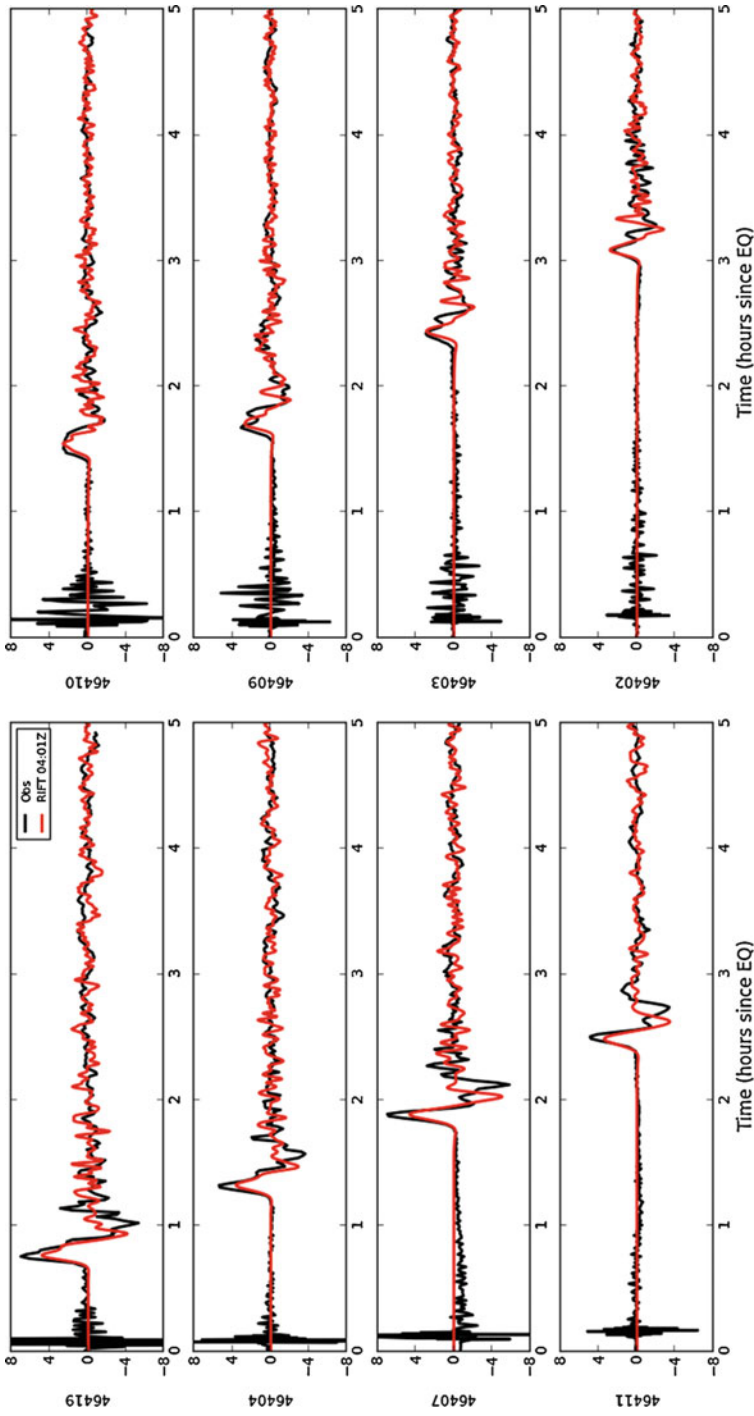
Earthquake Source Parameters, Rapid Estimates for Tsunami Forecasts and Warnings, Fig. 14 Energy (maximum wave amplitude) maps for the April 11, 2012, Northern Sumatra tsunami. (a) Forecast based on PTWC’s initial $M_w = 8.66$, (b) forecast based on PTWC W-phase CMT ($M_w = 8.78$), and (c) forecast based on USGS W-phase CMT ($M_w = 8.57$)

mechanism. The bottom panel (Fig. 14c) shows the maximum wave amplitude for the RIFT model solution using the USGS W-phase CMT ($M_w = 8.57$), obtained 1 h 40 min after the earthquake’s origin time. The maximum forecasted coastal wave amplitude barely reached 1 m. This

forecast combined with the sea-level observations allowed the PTWC to cancel the basin-wide tsunami watch sooner than would have been possible without the forecast. This event demonstrates the usefulness of obtaining an accurate focal mechanism for tsunami forecasting and the associated problems with magnitude-based tsunami warnings. Although we cannot yet avoid magnitude-based warnings for near field coastal populations, knowing the focal mechanism of the earthquake allows more accurate tsunami forecasting for the far field.

The October 28, 2012, 3:04 UTC Haida Gwaii, British Columbia, Canada, magnitude 7.7 earthquake provided another example of the usefulness of the CMT derived from the W-phase inversion for real-time tsunami forecasting. Historically, this region has been characterized by strike-slip earthquakes. This event, however, had a thrust mechanism, as shown by the W-phase CMT solution. Figure 15 shows a comparison of observations at DARTs (deep ocean bottom pressure sensors) with RIFT forecasts obtained 57 min after the earthquake origin time, based on the USGS W-phase CMT ($M_w = 7.7$). The forecast was reasonably good across the basin, although in the near field, the forecast underestimated the wave amplitudes. We note that at the time of the forecast, no DART stations had yet recorded a complete waveform of the tsunami.

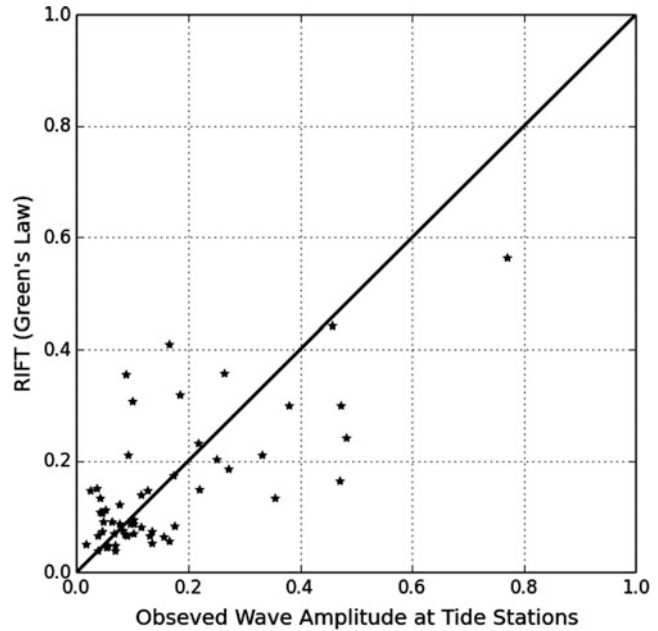
Figure 16 compares observations obtained for the Haida Gwaii event from 57 tide stations throughout the Pacific with RIFT forecast generated at 0401Z. Although there is considerable scatter between the observed and predicted wave amplitudes (defined as an average of maximum zero to peak and maximum zero to trough amplitudes), the mean ratio between the predicted and observed wave amplitudes is 1.4, or prediction is within a factor of two of the observed. If only tide stations that are more exposed to the open ocean are included (38 out of 57 tide stations), then the mean ratio is 1.07. We note that tsunami warning cannot be based on forecast at tide stations. For example, during the 2009 Samoa tsunami, post-event survey showed run-up reaching 7 m on the island of Tutuila in American Samoa, but the tide station in Pago Pago Harbor only recorded a



Earthquake Source Parameters, Rapid Estimates for Tsunami Forecasts and Warnings, Fig. 15 Comparison of tsunami recorded at DARTs across the Pacific with RIFT forecast based on USGS W-phase CMT (Mw = 7.7). The DART buoy locations and data can be found at: <http://www.ndbc.noaa.gov/>. (October 28, 2012, Haida Gwaii tsunami)

Earthquake Source Parameters, Rapid Estimates for Tsunami Forecasts and Warnings,

Fig. 16 Comparison of observed wave amplitudes at tide stations with RIFT forecast based the USGS W-phase CMT. Wave amplitude is defined as the average of maximum zero to peak and maximum zero to trough wave amplitudes. (October 28, 2012, Haida Gwaii tsunami)



maximum wave amplitude of $\sim 2\text{m}$. In summary, the W-phase CMT method combined with a linear shallow water model and the Green's law can provide useful and rapid guidance for tsunami warning, complementing existing database approaches. Real-time inundation forecasting based on propagation forecast results obtained using the CMT obtained by inversion of the W-phase can also be added in the future.

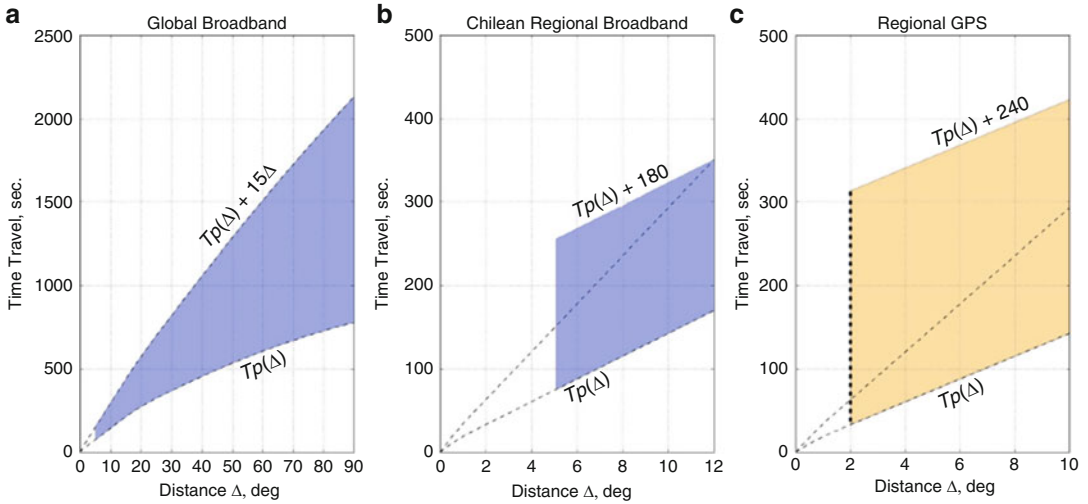
Future Directions

Given the availability of high-quality broadband seismic data, the tsunami warning centers can determine basic earthquake source parameters rapidly. However, the source characterization at the warning centers has rested largely on scalar measures of earthquake magnitude. The reasons for this are historical and practical. The warning centers have not always received the quantity and quality of seismic data that they do now, and in the interest of speed, the calculation of scalar measures can be accomplished with the data at hand in a small amount of time. One issue that the PTWC faced during the 2004 Sumatra earthquake was that no near real-time magnitude method existed

at the time that would correctly estimate the size of the Sumatra earthquake. Since then, new techniques have been developed to determine the magnitude of great earthquakes. Among these are techniques are the W-phase source inversion method (Kanamori 1993; Kanamori and Kikuchi 1993; Cummins 1997; Kanamori and Rivera 2008).

Luis Rivera, Zacharie Duputel, and PTWC scientists implemented the W-phase method (Kanamori and Rivera 2008) at the PTWC in late 2010, using data from seismic stations in the 5 to 50 degree epicentral range. The first W-phase CMT and unsaturated M_w estimate are therefore available at 25 to 30 min after earthquake origin time.

Using data from the Earthquake Research Institute F-net, for eight large Japanese earthquakes, Kanamori H. and Rivera L. (Kanamori et al. 2008) showed that, because the W-phase includes the complete wave field, including both near- and far-field displacements (Cummins 1997), it could be used for regional tsunami warnings, reducing its availability for tsunami from approximately 25 to 6 min after earthquake origin time. They achieved this with only minor modifications to the algorithm:



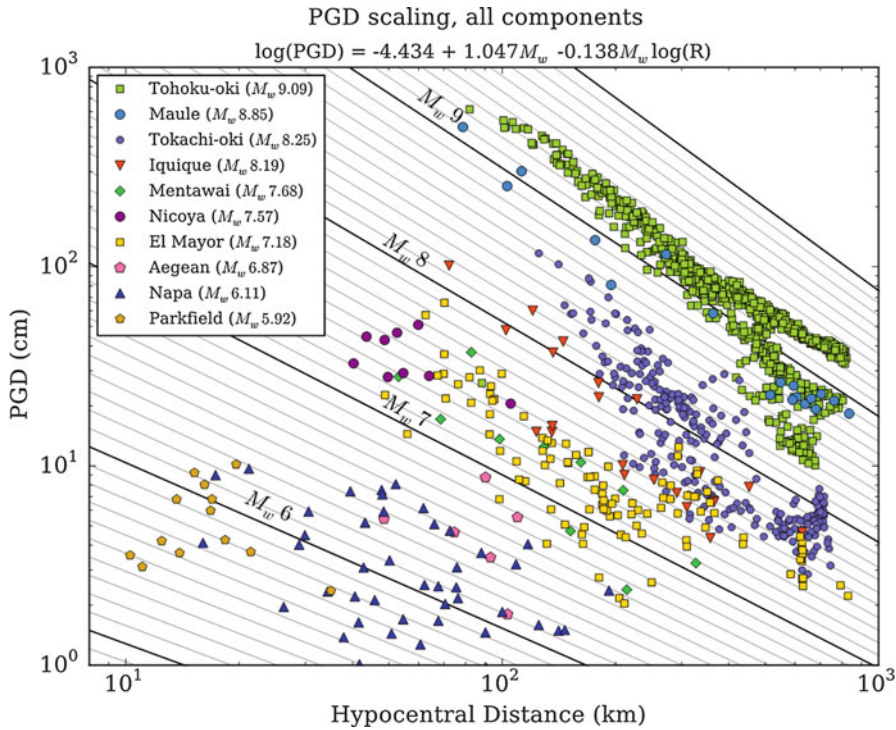
Earthquake Source Parameters, Rapid Estimates for Tsunami Forecasts and Warnings, Fig. 17 Time window comparison between (a) teleseismic W-phase inversion from seismic data, (b) regional inversion from seismic data, and (c) regional inversion using GPS data. (a) shows a

window from $T_p(\Delta)$ to $T_p(\Delta) + 15\Delta$, where Δ is the station to centroid distance in degrees from 5° to 90° ; (b) shows a constant window of 180 s with Δ between 5° and 12° distance; and (c) shows a constant window of 240 s for Δ between 2° and 10° . (Fig. 2. from Riquelme et al. 2016)

1. Using the teleseismic windowing scheme (see Fig. 17a), the duration of the data becomes too short at short distances. Thus, Kanamori and Rivera (Kanamori et al. 2008) used a constant window with a duration of $15\Delta_0$ where Δ_0 is a fixed distance, 12° . In this case the record duration is 180 s (see Fig. 17b).
2. The records are often clipped very early at short distances; thus, Kanamori and Rivera (Kanamori et al. 2008) removed all of the stations at distances shorter than 5° from their W-phase inversion. Also, they used a maximum epicentral distance of 12° , which provided W-phase-based moment tensor solution 6 min after the earthquake's origin time.
3. For regional applications, one often needs to determine the source mechanism of smaller earthquakes, down to Mw 6. Thus, Kanamori and Rivera (Kanamori et al. 2008) used, in addition to their standard frequency band (Kanamori and Rivera 2008), slightly shorter frequency bands, such as 0.00167 Hz (600 s) to 0.005 Hz (200 s) or 0.002 Hz (500 s) to 0.01 Hz (100 s), depending on the noise level of the available data.

Hayes et al. (2009) implemented the W-phase technique at the USGS and extended it to lower magnitudes. Duputel, Z. (Duputel et al. 2011, 2012) calculated W-phase moment tensors for all earthquakes worldwide above 6.5 from 1990 to 2012 and recalculated new filters for different magnitudes. Rivera et al. (2011) and Riquelme et al. (2016) extended the algorithm to regional data from high-rate GPS data (see Fig. 17c). They demonstrated that inverting for the W-phase CMT using high-rate, continuous cGPS data from stations within 5° from the earthquake source would provide a full moment tensor within 5 min of rupture initiation, depending on the number of stations and azimuthal coverage. Regional implementations are also operating in Japan, Mexico, Australia, Taiwan, and in China. PTWC scientists are currently testing the W-phase inversions from data obtained within 30 degrees epicentral distance, in order to obtain the W-phase CMT and Mw within 15 min of earthquake origin time.

In addition to size, source mechanism, and source duration, the warning centers are interested in more detailed properties of the source such as direction of rupture and the distribution of slip along the fault. This information is important as



Earthquake Source Parameters, Rapid Estimates for Tsunami Forecasts and Warnings, Fig. 18 Scaling of peak ground displacement (PGD) measurements. The

oblique lines are the predicted scaling values from the L1 regression of the PGD measurements as a function of hypocentral distance. (Figure 2 from Melgar 2015)

it can be used in tsunami wave height forecast models to better their predictions.

In the near future, the tsunami warning centers will incorporate finite-fault modeling. Finite-fault modeling involves the inversion of seismic waveforms to recover more detailed information about the source process including the slip distribution, rupture propagation speed, and moment release history (Ammon et al. 2005; Giovanni et al. 2002; Hartzell and Heaton 1986; Hartzell and Mendoza 1991; Mendoza 1996; Wald et al. 1990).

Weinstein and Lundgren (2008) explored the potential of a simple teleseismic P-wave inverse method for the rupture history of an earthquake for use in a tsunami warning center context. The calculations proceed quickly enough that a slip distribution may be available just a few minutes after a suitable set of P-waveforms are obtained. Hence finite-fault modeling results can be used in tsunami wave height forecast models to provide a timely initial estimate of tsunami wave heights.

Using the seismic data available within the first 5 min after rupture initiation, tsunami warning centers may significantly underestimate the magnitude of great Mw 9 plus earthquakes such as the Mw 9.2 Sumatra 2004 event, complex events such as the Mw 8.4 Peru 2001 earthquake, and “tsunami earthquakes” such as the 1992 Nicaragua and 2006 Java earthquakes, leading to inaccurate tsunami forecasts for those most threatened by the resulting tsunami (Figs. 4, 5, and 6).

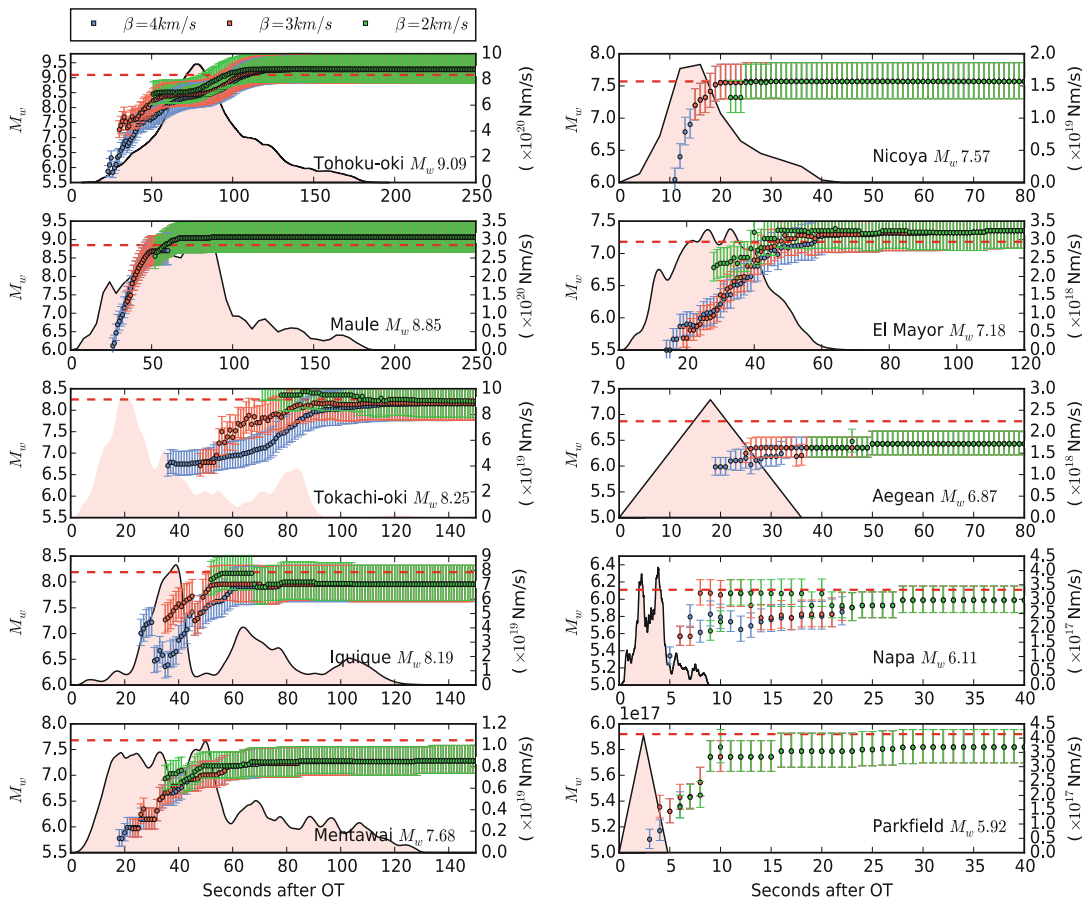
Global Navigation Satellite System (GNSS) displacement data and seismogeodetic (Bock et al. 2011) in the near field will enable tsunami warnings within 3–4 min after initiation of rupture at the hypocenter (Melgar et al. 2016). Real-time source modeling codes already provide unsaturated estimates of moment magnitude from peak ground displacement (PGD) (Crowell et al. 2013; Melgar and Crowell 2013; Melgar et al. 2015), centroid moment tensors (Melgar et al. 2012; Melgar and Crowell 2013; Rivera et al. 2011;

Riquelme et al. 2016), and fault slip inversions (Crowell et al. 2012; Melgar and Crowell 2013; Melgar et al. 2016), within 1–2 min of rupture initiation (Figs. 18, 19 and 20). This source information can then drive PTWC’s real-time tsunami forecasting model (RIFT) (Duputel et al. 2011; Fryer et al. 2010; Savage 1972; Scholz 1982; Wang et al. 2012), generating forecasts of expected tsunami amplitudes at the near-source coasts within 3–4 min of earthquake origin time (Melgar et al. 2016).

NASA/JPL, the Scripps Institute of Oceanography (SIO), Central Washington University (CWU), University of Oregon, and the University

of Washington (UW), with funding and guidance from NASA and leveraging the USGS funded ShakeAlert development, are providing this data and source characterization algorithms to the NOAA National Tsunami Warning Center (NTWC) and to the Pacific Tsunami Warning Center (PTWC).

In the first 2 years of this work, we have established and deployed an Earthworm architecture (GWORM) for this data movement for the algorithms. We have also installed modules for estimating moment magnitude (M_w) from peak ground displacement (PGD), within 2–3 min of the event, computing coseismic displacements



Earthquake Source Parameters, Rapid Estimates for Tsunami Forecasts and Warnings, Fig. 19

Retrospective analysis of the time evolution of magnitude using the scaling law of equation (1) from Melgar et al. (2015). Plotted are the magnitude calculations using three travel time masks at 2, 3, and 4 km/s. The error

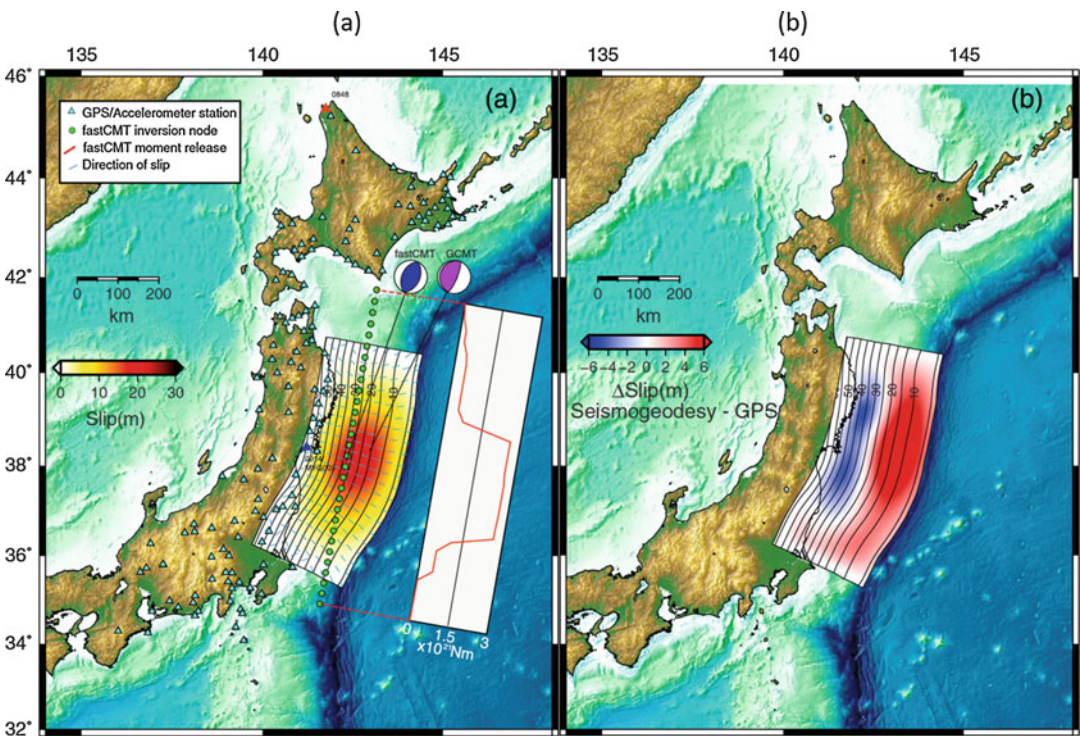
bars are determined using the uncertainties of the regression coefficients. The red dashed line is the magnitude from the slip inversion for that event. The shaded pink regions are the source time functions for the kinematic slip inversions. (Figure 4. From Melgar 2015)

converging to static offsets and visualization tools. These modules are being installed in the TWC’s operational framework and will be tested using both historical data recordings and new events as they occur.

Global Navigation Satellite System (GNSS) data, and the real-time earthquake source modeling codes which rely on it, will provide unsaturated estimates of moment magnitude, centroid moment tensor solutions, and fault slip models to NOAA’s tsunami warning centers within a few minutes after earthquake initiation. These earthquake source characterizations will drive

tsunami models such as RIFT (Duputel et al. 2011; Fryer et al. 2010; Savage 1972; Scholz 1982; Wang et al. 2012) (discussed above), enabling tsunami warnings within 3–5 min after earthquake origin time for coastal populations in the near field, where over 80% of tsunami-related casualties would otherwise occur.

Acknowledgments We thank Paula Dunbar of the National Geophysical Data Center for helping us obtain the data we needed and IRIS without which most of this work let alone a functioning TWC would not be possible. We also thank the PTWC for use of its facilities in preparing this manuscript.



Earthquake Source Parameters, Rapid Estimates for Tsunami Forecasts and Warnings, Fig. 20 CMT and slip inversions from seismogeodetic data (GNSS and seismic data combined via Kalman filter). (a) “fastCMT” and slip inversion results from GNSS data only. Green circles are the point sources superimposed to compute the line source of CMT solutions, the final averaged solution shown as fastCMT, and the Global CMT solution (GCMT) shown for comparison. The inset shows the moment release from the line source as a function of distance along fault. Shown along the fault interface with 10 km depth contours from the

Slab 1.0 model (Hayes et al. 2011) is the result of the slip inversion; the blue lines represent the direction of slip. The triangles indicate the locations of all the GPS/accelerometer stations used for computing the slip inversion and CMT solution. (b) Difference between slip inversions computed using seismogeodetic displacements compared to the inversion carried out using the GPS-only derived displacements. Red indicates more slip with the seismogeodetic solution, and blue indicates more slip with the GPS-only solution. (Fig. 2 from Melgar et al. 2013)

Bibliography

Primary Literature

- Aki K (1966) Generation and propagation of G waves from the Niigata earthquake of June 16, 1964, Part 2. Estimation of earthquake moment, from the G wave spectrum. *Bull Earth quake Res Inst Tokyo Univ* 44:73–88
- Aki K (1967) Scaling law of seismic spectrum. *J Geophys Res* 72:1217–1231
- Allen RV (1978) Automatic earthquake recognition and timing from single traces. *Bull Seism Soc Am* 68:1521–1532
- Allen RV (1982) Automatic phase pickers: their present use and future prospects. *Bull Seism Soc Am* 72:225–242
- Ammon CJ, Ji C, Thio HK, Robinson D, Sidao N, Hjorleifsdottir V, Kanamori H, Lay T, Das S, Helmlinger D, Ichinose G, Polet J, Wald D (2005) Rupture process of the 2004 Sumatra–Andaman earthquake. *Science* 6:113–1139
- Arakawa A, Lamb V (1977) Computational design of the basic dynamical processes of the UCLA general circulation model. *Methods Comput Phys* 17:174–267
- Becker JJ, Sandwell DT, Smith WHF, Braud J, Binder B, Depner J, Fabre D, Factor J, Ingalls S, Kim S-H, Ladner R, Marks K, Nelson S, Pharaoh A, Trimmer R, Von Rosenberg J, Wallace G, Weatherall P (2009) Global Bathymetry and Elevation Data at 30 Arc Seconds Resolution: SRTM30_PLUS. *Marine Geodesy* 32(4):355–371. <https://doi.org/10.1080/01490410903297766>
- Bilek SL, Lay T (1999) Rigidity variations with depth along interplate megathrust faults in subduction zones. *Nature* 400:443–446
- Bilek SL, Ruff LJ (2002) Analysis of the 23 June 2001 *M*_W 8.4 Peru underthrusting earthquake and its aftershocks. *Geophys Res Lett* 8:21:1–21:4
- Bilek SL, Lay T, Ruff LJ (2004) Radiated seismic energy and earthquake source duration variations from teleseismic source time functions for shallow subduction zone thrust earth-quake. *J Geophys Res* 109:B09308
- Boatwright J, Choy GL (1986) Teleseismic estimates of the energy radiated by shallow earthquakes. *J Geophys Res* 91:2095–2112
- Boatwright J, Choy GL, Seekins LC (2002) Regional estimates of radiated seismic energy. *Bull Seism Soc Am* 92:1241–1255
- Bock Y, Melgar D, Crowell BW (2011) Real-time strong-motion broadband displacements from collocated GPS and accelerometers. *Bull Seismol Soc Am* 101:2904–2925. <https://doi.org/10.1785/0120110007>
- Bormann P, Baumbach M, Bock G, Grosser H, Choy GL, Boatwright J (2002) Seismic sources and source parameters. In: Bormann P (ed) IASPEI new manual seismological observatory practice, vol 1. Chapter 3. GeoForschungsZentrum Potsdam, pp 1–94. (This can also go as in the text cited review paper)
- Bormann P, Wylegalla K (2005) Quick estimator of the size of great earthquakes. *Eos Trans AGU* 86(46):464
- Bormann P, Wylegalla K, Saul J (2006) Broadband body-wave magnitudes *m*_B and *m*_{BC} for quick reliable estimation of the size of great earthquakes. USGS Tsunami Sources Work- shop 2006, poster, http://spring.msi.umn.edu/USGS/Posters/Bormann_etal_poster.pdf
- Bormann P, Saul J (2008a) Earthquake magnitude. In: Meyers A (ed) *Encyclopedia of complexity and systems science*. Springer, Heidelberg
- Bormann P, Saul J (2008b) The new IASPEI standard broadband magnitude *m*_B. *Seism Res Lett* 79:698–705
- Brune J (1970) Tectonic stress and seismic shear waves from earthquakes. *J Geophys Res* 75:4997–5009
- Brune J (1971) Tectonic stress and seismic shear waves from earthquakes; Correction. *J Geophys Res* 76:5002
- Bryant E (2001) Distribution and fatalities. In: Bryant E (ed) *Tsunami: the underrated hazard*. School of Science and the Environment, Coventry University, Coventry. Cambridge University Press, Cambridge, pp 15–24
- Choy GL, Boatwright J (2007) The energy radiated by the 26 December 2004 Sumatra–Andaman earthquake estimated from 10-minute P-wave windows. *Bull Seism Soc Am* 97:S18–S24
- Crowell BW, Bock Y, Melgar D (2012) Real-time inversion of GPS data for finite fault modeling and rapid hazard assessment. *Geophys Res Lett* 39:L09305. <https://doi.org/10.1029/2012GL051318>
- Crowell BW, Melgar D, Bock Y, Haase JS, Geng J (2013) Earthquake magnitude scaling using seismogeodetic data. *Geophys Res Lett* 40:6089–6094. <https://doi.org/10.1002/2013GL058391>
- Cummins PR (1997) Earthquake near field and W phase observations at teleseismic distances. *Geophys Res Lett* 24:2857–2860
- Duputel Z, Rivera L, Kanamori H, Hayes GP, Hirshorn B, Weinstein S (2011) Real-time W-phase inversions during the 2011 Tohoku-oki earthquake. *Earth Planets Space* 63(7):535–539
- Duputel Z, Rivera L, Kanamori H, Hayes GH (2012) W phase source inversion for moderate to large earthquakes (1990–2010). *Geophy J Int* 189:1125–1147
- Ebeling C, Okal E (2012) An extension of the E/M0 tsunami earthquake discriminant Theta to regional distances. *Geophys J Int* 190(3):1640–1656
- Evans JR, Allen S (1983) A teleseism-specific detection algorithm for single short-period traces. *Bull Seism Soc Am* 73:1173–1186
- Foster JH, Brooks BA, Wang D, Carter GS, Merrifield MA (2012) Improving Tsunami Warning Using Commercial Ships. *Geophys Res Lett* 39:L09603. <https://doi.org/10.1029/2012GL051367>
- Fryer G, Hirshorn B, McCreery S, Cessaro RK, Weinstein S (2005) Tsunami warning in the near field: the approach in Hawaii. *EOS* 86:S44B-04
- Fryer G, Holschuh ND, Wang D, Becker N (2010) In: Improving tsunami warning with a rapid linear model, Abstract NH33A-1378 presented at 2010 fall meeting. AGU, San Francisco, 13–17 Dec

- Fukao Y (1979) Tsunami earthquakes and subduction processes near deep-sea trenches. *J Geophys Res* 84:2303–2314
- Geller RJ, Kanamori H (1977) Magnitudes of great shallow earthquakes from 1904 to 1952. *Bull Seismol Soc Am* 67:587–598
- Gica E, Spillane VTMC, Chamberlin C, Newman J (2008) In: Development of the forecast propagation database for NOAA's Short-term Inundation Forecast for Tsunamis (SIFT). NOAA Technical Memorandum OAR PMEL-139, Pacific Marine Environmental Laboratory, Seattle, p 95
- Giovanni MK, Beck SL, Wagner L (2002) The June 23, 2001 Peru earthquake and the southern Peru subduction zone. *Geophys Res Lett* 29:14:1–14:4
- Global Centroid Moment Tensor Catalog, <http://www.globalcmt.org>
- Gower J (2005) Jason 1 detects the 26 December 2004 tsunami. *Eos Trans AGU* 86(4):37–38
- Gutenberg B (1945a) Amplitudes of surface waves and magnitudes of shallow earthquakes. *Bull Seism Soc Am* 35:3–12
- Gutenberg B (1945b) Amplitudes of P, PP, and S, and magnitudes of shallow earthquakes. *Bull Seism Soc Am* 35:57–69
- Gutenberg B (1945c) Magnitude determinations of deep-focus earthquakes. *Bull Seism Soc Am* 35:117–130
- Gutenberg B, Richter CF (1956a) Earthquake magnitude, intensity, energy and acceleration. *Bull Seism Soc Am* 46:105–145
- Gutenberg B, Richter CF (1956b) Magnitude and energy of earthquakes. *Annali di Geofisica* 9:1–15
- Hanks T, Kanamori H (1979) A moment magnitude scale. *J Geophys Res* 84:2348–2350
- Hara T (2007a) Measurement of the duration of high-frequency radiation and its application to determination of the magnitudes of large shallow earthquakes. *Earth Planets Space* 59:227–231
- Hara T (2007b) Magnitude determination using duration of high frequency energy radiation and displacement amplitude: application to tsunami earthquakes. *Earth Planets Space* 59:561–565
- Hartzell S, Heaton T (1986) Rupture history of the 1984 Morgan Hill, California, earthquake from the inversion of strong motion records. *Bull Seism Soc Am* 76:649–674
- Hartzell S, Mendoza C (1991) Application of an iterative least-squares waveform inversion of strong-motion and teleseismic records to the 1978 Tabas, Iran earthquake. *Bull Seism Soc Am* 81:305–331
- Hayes GP, Rivera L, Kanamori H (2009) Source inversion of the W-Phase: real-time implementation and extension to low magnitudes. *Seismol Res Lett* 80(5):817–822
- Hayes GP, Earle PS, Benz HM, Wald DJ, Briggs R, The USGS/NEIC Earthquake Response Team (2011) 88 hours: the U.S. Geological survey national earthquake information center response to the March 11, 2011 Mw 9.0 Tohoku earthquake. *Seismol Res Lett* 82(4):481–493
- Henry C, Das S (2001) Aftershock zones of large shallow earthquakes: fault dimensions, aftershock area expansion and scaling relations. *Geophys J Int* 147:272–293
- Hirshorn B, Lindh A, Allen R (1987) Real time signal duration magnitudes from low-gain short period seismometers. *USGS OFR* 87:630
- Hirshorn B, Lindh G, Allen RV, Johnson C (1993) Real time magnitude estimation for a prototype early warning system (EWS) from the P-wave, and for earthquake hazards monitoring from the coda envelope. *Seis Res Lett* 64:48
- Hirshorn B, Weinstein S, Tsuboi, S. (2013). On the application of Mwp in the near field and the March 11, 2011 Tohoku earthquake. *Pure Appl Geophys* 170 (6–8):975–991. <https://doi.org/10.1007/s00024-012-0495-3>
- Hirshorn B (2004) Moment magnitudes from the initial P-wave for local tsunami warnings. *Seism Res Lett* 74:272–273
- Hirshorn B (2007) The Pacific tsunami warning center response to the Mw6.7 Kiholo Bay earthquake and lessons for the future. *Seism Res Lett* 78:299
- Hoechner A, Ge M, Babeyko Y, Sobolev SV (2013) Instant tsunami early warning based on real-time GPS – tohoku 2011 case study. *Nat Hazards Earth Syst Sci* 13:1285–1292
- Houston H, Kanamori H (1986) Source spectra of great earthquakes, teleseismic constraints on rupture process and strong motion. *Bull Seism Soc Am* 76:19–42
- Imamura F (1996) Review of tsunami simulation with a finite difference method. In: Yeh H, Liu P, Synolakis C (eds) Long-wave runup models. World Scientific, Singapore, pp 25–42
- Ishii M, Shearer PM, Houston H, Vidale JE (2005) Extent, duration and speed of the 2004 Sumatra–Andaman earthquake imaged by the Hi-Net array. *Nature* 435:933–936
- Johnson CE, Lindh A, Hirshorn B (1994) Robust regional phase association. *US Geol Surv Open-File Rep* 94:621
- Johnson CE, Bittenbinder A, Bogaert B, Dietz L, Kohler W (1995) Earthworm: a flexible approach to seismic network processing. *IRIS Newslett XIV* 2:1–4
- Kamigaichi O (2009) Tsunami forecasting and warning. In: Meyers RA (ed) *Encyclopedia of Complexity and Systems Science*. Springer, Heidelberg, pp 9592–9618
- Kanamori H (1972) Mechanism of tsunami earthquakes. *Phys Earth Planet Inter* 6:246–259
- Kanamori H (1977) The energy release in great earthquakes. *J Geophys Res* 82:2981–2987
- Kanamori H (1978) Quantification of earthquakes. *Nature* 271:411–414
- Kanamori H (1983) Magnitude scale and quantification of earthquakes. *Tectonophysics* 93:185–199
- Kanamori H (1993) W Phase. *Geophys Res Lett* 20:1691–1694

- Kanamori H, Kikuchi M (1993) The 1992 Nicaragua earthquake: a slow tsunami earthquake associated with subducted sediment. *Nature* 361:714–715
- Kanamori H (2006) Seismological aspects of the December 2004 great Sumatra Andaman earthquake. *Earthquake Spectra* 22:S1–S12
- Kanamori H, Rivera L (2008) Source inversion of W phase – speeding up tsunami warning. *Geophys J Int* 175:222–238
- Kanamori H, Rivera L, Earthquake Research Institute (2008) Application of the W phase source inversion method to regional tsunami 1 Seismological Lab, California Institute of Technology, Pasadena, University of Tokyo
- Kikuchi M, Yamanaka Y (2001) EIC Seismological Note Number 105, www.eic.eri-u-tokyo.ac.jp/EIC/EIC_news/105E.html
- Krüger F, Ohrnberger M (2005) Tracking the rupture of the Mw9.3 Sumatra earthquake over 1150 km at teleseismic distance. *Nature* 435:937–939
- Kowalik Z, Whitmore PM (1991) An investigation of two tsunamis recorded at Adak, Alaska. *Sci Tsunami Haz* 9:67–84
- Lamb H (1932) *Hydrodynamics*, 6th edn. Dover Publications, New York
- Lay T, Kanamori H, Ammon C et al (2005) The Great Sumatra – Andaman earthquake of 26 December 2004. *Science* 308:1127–1133
- Lockwood OG, Kanamori H (2006) Wavelet analysis of the seismograms of the 2004 Sumatra–Andaman earthquake and its application to tsunami early warning. *Geochem Geophys Geosyst* 7:Q09013. <https://doi.org/10.1029/2006GC001272>
- Lomax A, Michelini A, Piatanesi A (2007) An energy-duration procedure for rapid determination of earthquake magnitude and tsunamigenic potential. *Geophys J Int* 170:1195–1120
- Lomax A, Michelini A (2008) Mw_{pd}: A duration-amplitude procedure for rapid determination of earthquake magnitude and tsunamigenic potential from P waveforms. *Geophys J Int*. <https://doi.org/10.1111/j.1365-246X.2008.03974>
- Lomax A, Michelini A (2012) Tsunami early warning within 5–10 minutes. *Pure Appl Geophys* 169. <https://doi.org/10.1007/s00024-012-0512-6>
- Melgar D, Bock Y, Crowell BW (2012) Real-time centroid moment tensor determination for large earthquakes from local and regional displacement records. *Geophys J Int* 188:703–718. <https://doi.org/10.1111/j.1365-246X.2011.05297.x>
- Melgar D, Crowell BW, Bock Y, Haase JS (2013) Rapid modeling of the 2011 Mw 9.0 Tohoku-oki earthquake with seismogeodesy. *Geophys Res Lett* 40:1–6
- Melgar D, Crowell BW, Geng J, Allen RM, Bock Y, Riquelme S, Hill EM, Protti M, Ganas A (2015) Earthquake magnitude calculation without saturation from the scaling of peak ground displacement. *Geophys Res Lett* 42:5197–5205. <https://doi.org/10.1002/2015GL064278>
- Melgar D et al (2016) Local tsunami warnings: perspectives from recent large events. *Geophys Res Lett* 43:1109–1117. <https://doi.org/10.1002/2015GL067100>
- Mendoza C (1996) Rapid derivation of rupture history for large earthquakes. *Seismol Res Lett* 67:19–26
- NOAA Special Report (2012) Proceedings and results of the 2011 NTHMP model benchmarking workshop, Department of Commerce and Texas A&M University at Galveston, p 437
- Newman AV, Okal EA (1998) Teleseismic estimates of radiated seismic energy: the E/M0 discriminant for tsunami earthquakes. *J Geophys Res* 103:26885–26898
- Okada Y (1985) Surface deformation due to shear and tensile faults in a half space. *Bull Seismol Soc Am* 75:1135–1154
- Okal EA, Talandier J (1989) M_m: a variable-period mantle magnitude. *J Geophys Res* 94:4169–4193
- Okal EA (1992a) Use of mantle magnitude *M_m* for reassessment of the moment of historical earthquakes-I: Shallow events. *PAGEOPH* 139:17–57
- Park J, Song TA, Tromp J, Okal E, Stein S, Roullet G, Clevede E, Laske G, Kanamori H, Davis P, Berger J, Braitenberg C, Camp MV, Xiang'e L, Heping S, Houze X, Rosat S (2005) Earth's free oscillations excited by the 26 December 2004 Sumatra–Andaman earthquake. *Science* 20:1139–1144
- Richter CF (1935) An instrumental earthquake magnitude scale. *Bull Seism Soc Am* 25:1–32
- Rivera LA, Kanamori H, Duputel Z (2011) W phase source inversion using the high-rate regional GPS data of the 2011 Tohoku oki earthquake, in AGU fall meeting abstracts, vol 1, p 4
- Riquelme S, Bravo F, Melgar D, Benavente R, Geng J, Barrientos S, Campos J (2016) W phase source inversion using high-rate regional GPS data for large earthquakes. *Geophys Res Lett* 43(7):3178–3185
- Satake K (1994) Mechanism of the 1992 Nicaragua tsunami earthquake. *Geophys Res Lett* 21:2519–2522
- Savage JC (1972) Relation of corner frequency to fault dimensions. *J Geophys Res* 77:3788–3795
- Scholz C (1982) Scaling laws for large earthquakes: consequences for physical models. *Bull Seism Soc Am* 72:1–14
- Seno T, Hirata K (2007) Did the 2004 Sumatra–Andaman earthquake involve a component of tsunami earthquakes? *Bull Seism Soc Am* 97:S296–S306
- Stein S, Okal EA (2007a) Ultralong period seismic study of the December 2004 Indian Ocean earthquake and implications for regional tectonics and the subduction process. *Bull Seism Soc Am* 97:279–295
- Stein S, Okal EA (2007b) Ultralong Period Seismic Study of the December 2004 Indian Ocean earthquake and implications for regional tectonics and the subduction process. *Bull Seism Soc Am* 97:S279–S295
- Tatehata H (1997) The new tsunami warning system of the Japan meteorological agency. In: Hebenstreit G (ed) *Perspectives on tsunami hazard reduction*. Kluwer, Dordrecht, pp 175–188

- Tsuboi SK, Abe K, Takano K, Yamanaka Y (1995) Rapid determination of Mw from broadband P waveforms. *Bull Seism Soc Am* 83:606–613
- Tsuboi S, Whitmore PM, Sokolowski TJ (1999) Application of Mwp to deep and teleseismic earthquakes. *Bull Seism Soc Am* 89:1345–1351
- Vanek J, Zatopek A, Karnik V, Kondorskaya N, Ryzhichenko Y, Savarenski S, Solovov S, Shebalin N (1962) Standardization of magnitude scales. *Izv Acad Sci USSR Geophys Ser*:108–111. English translation
- Vassiliou MS, Kanamori H (1982) The energy release in earth-quakes. *Bull Seism Soc Am* 72:371–387
- Wald DJ, Helmberger DV, Hartzell S (1990) Rupture process of the 1987 Superstition Hills earthquake from the inversion of strong-motion data. *Bull Seism Soc Am* 80:1079–1098
- Wang D, Walsh D, Becker N, Fryer G (2009) A methodology for tsunami wave propagation forecast in real time, *EOS Trans AGU*, 90(52), Fall Meet. Suppl., Abstract OS43A-1367
- Wang D, Becker NC, Walsh D, Fryer G, Weinstein S, McCreery C, Sardina V, Hsu V, Hirshorn B, Hayes G, Duputel Z, Rivera L, Kanamori H, Koyanagi K, Shiro B (2012) Real-time forecasting of the April 11, 2012 Sumatra Tsunami. *Geophys Res Lett* 39:L19601. <https://doi.org/10.1029/2012GL053081>
- Weinstein SA, McCreery C, Hirshorn B, Whitmore P (2005) Comment on “A strategy to rapidly determine the magnitude of great earthquakes” by Menke W, Levin V. *Eos* 86:263
- Weinstein SA, Okal EA (2005) The mantle magnitude Mm and the slowness parameter 8: five years of real-time use in the context of tsunami warning. *Bull Seism Soc Am* 95:779–799
- Weinstein SA, Lundgren PL (2008) Finite fault modeling in a tsunami warning center context. In: Tiampo KF, Weatherley DK, Weinstein SA (eds) *Earthquakes: simulations, sources and tsunamis*. Birkhauser, Basel
- Wells DL, Coppersmith KJ (1994) New empirical relationships among magnitude, rupture length, rupture width, rupture area, and surface displacement. *Bull Seism Soc Am* 84:974–1002
- Wessel P (2009) Analysis of observed and predicted tsunami travel times for the Pacific and Indian Oceans. *Pure Appl Geophys* 166:301–324. <https://doi.org/10.1007/s00024-008-0437-2>
- Wessel P, Smith WHF (1991) Free software helps map and display data. *Eos Trans AGU* 72:441
- Whitmore PM, Sokolowski TJ (2002) Automatic earthquake processing developments at the US West Coast/Alaska tsunami warning center. *Recent Research Developments in Seismology*, pp 1–13, Kervala: Transworld Research Net- work. ISBN 81-7895, 072-3
- Whitmore PM, Tsuboi S, Hirshorn B, Sokolowski TJ (2002) Magnitude-dependent correction for Mwp. *Sci Tsunami Hazards* J20:187–192
- Widjo K et al (2006) Rapid survey on tsunami Java July 17 2006. http://nctr.pmel.noaa.gov/java20060717/tsunami-java170706_e.pdf. Accessed July 2008
- Withers M, Aster R, Young C, Beiriger J, Harris M, Trujillo J (1998) A comparison of select trigger algorithms for automated global seismic phase and event detection. *Bull Seism Soc Am* 88:95–106
- Yasuda T, Mase H (2013) Real-time tsunami prediction by inversion method using offshore observed GPS buoy data: Nankaido. *J Waterway Port Coastal Ocean Eng* 139(3):221–231

Books and Reviews

- Abercrombie R, McGarr A, Di Toro G, Kanamori H (eds) (2006) *Earthquakes: radiated energy and the physics of faulting*. In: *Geophysical monographs* 170. American Geophysical Union, Washington, DC
- Aki K, Richards PG (1980) *Quantitative seismology theory and methods*, vol 2. W.H. Freeman Co, San Francisco
- Aki K, Richards PG (2002) *Quantitative seismology*, 2nd edn. University Science Books, Sausalito
- Båth M (1981) *Earthquake magnitude – recent research and current trends*. *Earth Sci Rev* 17:315–398
- Bormann P (ed) (2002) *IASPEI new manual of seismological observatory practice*, vol 1 and 2. Geoforschungszentrum, Potsdam, p 1250
- Duda S, Aki K (eds) (1983) *Quantification of earthquakes*. *Tectonophysics* 93. Special issue 3(4):183–356
- Kanamori H, Anderson DL (1975) Theoretical basis of some empirical relations in seismology. *Bull Seism Soc Am* 65(5):1073–1095
- Kanamori H (1994) *Mechanics of earthquakes*. *Annu Rev Earth Planet Sci* 22:307–237
- Kanamori H, Rivera L (2006) Energy partitioning during an earth-quake. In: Abercrombie R, McGarr A, Kanamori H, Di Toro G (eds) *Earthquakes: radiated energy and the physics of faulting*. *Geophysical monograph*, vol 170. American Geophysical Union, Washington, DC, pp 3–13
- Kanamori H, Brodsky E (2004) The Physics of earthquakes. *Rep Prog Phys* 67:1429–1496
- Kanamori H (2006) The diversity of the physics of earthquakes. *Proc Japan Acad Ser B* 80:297–316
- Lay T, Wallace TC (1995) *Modern global seismology*. Academic, San Diego
- Okal EA (1992b) A student’s guide to teleseismic body wave amplitudes. *Seism Res Lett* 63(N2):169–180
- Richter CF (1958) *Elementary seismology*. WH Freeman Co, San Francisco
- Stein S, Wysession M (2003) *An introduction to seismology, earthquakes, and earth structure*. Blackwell Publishing, Oxford